Engine performance and emissions from a fumigated hydrogen/ammonia compression ignition engine with a hydrogen peroxide pilot

Gregor Paterson [a], Efstathios-Al. Tingas [a,*], Yannis Hardalupas [b], Alexander M.K.P. Taylor [b]

[a] School of Computing, Engineering and the Built Environment, Edinburgh Napier University, Edinburgh, EH10 5DT, UK
[b] Mechanical Engineering Department, Imperial College London, London, SW7 2AZ, UK

A B S T R A C T

The study investigates, numerically, the potential use of introducing aqueous H_2O_2 as an ignition promoter in a statistically homogeneous NH_3/H_2 fuelled, medium speed (1250 rpm), 4-stroke, 1.3 litre cylinder displacement, mildly boosted CI engine with a compression ratio of 17.6:1. The H_2 is considered to be produced on-board from ammonia cracking. An extensive campaign is undertaken using the commercial stochastic reactor model, SRM Engine Suite, which allowed the modelling of temporal, temperature and spatial stratification in the cylinder. The engine performance, combustion phasing, maximum pressure rise rate and emissions (NOx, N_2O and unreacted NH_3) are investigated in view of: (i) the share of molecular hydrogen in the initial NH_3/H_2 mixture from 10 to 40 percent; (ii) the mass of aqueous H_2O_2 introduced from 0.1 to 16 mg; (iii) the start of injection (-10 to $+6$ CAD aTDC) and duration of injection (1, 4 and 8 CAD); (iv) the amount of exhaust gas recirculation (up to 30 percent by mass); (v) the share of energy from the H_2O_2 in the aqueous solution mixture at less than 0.5 percent of that in the main fuel; (vi) engine load corresponding to a variation in the equivalence ratio from 0.32 to 1.2 by changing the mass of the NH_3/H_2 mixture in the combustion chamber. A wide range of loads (evaluated against the engine's rated power when operated with diesel and at its rated boost levels) can be achieved (44%–93%) with the energy share of H_2O_2 being as little as equivalent to 2.7% vol% that of the main fuel, ammonia, which is introduced into the cylinder. This implies that the required storage volume of the H_2O_2 is low, at a few percent that of the main ammonia tank. NOx emissions peak between $\phi = 0.6-0.65$ and rapidly decrease as the equivalence ratio increases or decreases reaching values marginally above the Tier III standard at high loads (>90%) while ammonia slip and N_2O emissions are generally extremely low (10^{-12} mg for NH_3 and < 0.01 mg/kWh for N_2O).

1. Introduction

The global movement towards a more sustainable future is evident across all industries, and the maritime industry is no exception. As of 2018, the maritime industry was responsible for 2.89% of global greenhouse gas (GHG) emissions, accounting for 1,076 million tonnes of CO_2 [1–3]. This is mainly due to the transportation of the world's goods and products via ships, as well as travel and leisure vessels worldwide. In response, the International Maritime Organisation (IMO) has established increasingly strict regulations on emissions, with the ultimate goal of reducing GHG emissions [1,4,5]: (i) by at least 20%, striving for 30%, by 2030, compared to 2008; (ii) by at least 70%, striving for 80%, by 2040, compared to 2008; (iii) reach net-zero GHG emissions '...by or around, i.e. close to, 2050...'. In the UK, the government has recently published the Clean Maritime Plan (CMP), outlining the details of a strategy that aspires to make the UK ship register the

world leader in zero emission maritime operations [6,7]. To accomplish this goal, the CMP has certain ambitious milestones; for example, by 2025 all new vessels should be designed to have zero emission propulsion capabilities, and by 2035 low to zero emission marine fuel bunker options should be available across the UK. In addition to carbon emissions, the IMO has set new standards for non-carbon emissions such as sulphur oxides (SOx) and nitrogen oxides (NOx), which are also harmful to the environment. The IMO 2020 regulation mandates a stringent 0.5% sulphur content limit in all fuels and 0.1% in Emission Control Areas [8]. Furthermore, the International Convention for the Prevention of Pollution from Ships (MARPOL) introduced Regulation 13, a tiered NOx structure for new and existing ships based on size, speed, and build date. According to that regulation, ships constructed after 2016 must produce no more than 3.4 g/kWh of NOx at an engine speed of <130 rpm, with the limit decreasing as the engine speed increases ($9\times n^{-0.2}$, where n the engine speed in rpm) [9].

Currently, the main sources of maritime fuel are (very low sulphur) heavy fuel oil and diesel, which both produce substantial amounts of carbon dioxide, as well as other emissions, predominantly NOx, SOx and soot, which are detrimental to the environment. Such fuels are widely used in compression ignition (CI) engines where the ignition of the charge is controlled by the introduction of the fuel at an appropriate instant (measured in terms of crank angle degrees (CAD)). Reducing carbon emissions from fossil fuel combustion, while at the same time lowering NOx and SOx emissions, is a challenging task without the installation of a selective catalytic reduction (SCR) system or adequate after-treatment [10]. Therefore, there is a need for alternatives which emit fewer GHGs, with options such as ammonia (NH_3) and hydrogen (H_2) emerging as '*zero carbon*' fuels, and methanol (CH_3OH) and liquefied natural gas (LNG) being proposed and researched as '*low carbon fuels*'. [4,11,12]. Among these options, ammonia and LNG are currently attractive due to their established infrastructure and distribution systems. While not without substantial disadvantages, ammonia shows some promise as a future fuel in combustion engines due to its zero-carbon and zero-sulphur composition [6,13,14]. Furthermore it is attractive because of the possibility of its production by renewable sources and – relative to hydrogen in either liquid (cryogenic) or pressurised form – its high energy density [12,15–18].

Existing infrastructure for producing '*green*' ammonia is not sufficiently widespread to meet the potential future demand of the market. Presently, production relies on the Haber–Bosch process with hydrogen produced from steam reforming of hydrocarbons, which produces substantial GNG emissions [4,15,19–21]. However, the technology for producing so-called 'green' ammonia is advancing, and several methods are available. One common approach involves using electrolysis to produce hydrogen from water and air separation units for nitrogen, which is then combined using a 'green'-powered Haber–Bosch process [21,22]. Other methods, such as electrochemical ammonia synthesis, bio-electrochemical and photoelectrochemical ammonia synthesis, are also being explored, but production levels are still very low [15,19,21]. In any case, the production of green ammonia is dependent on the development of plentiful amounts of reliable energy generation from renewable sources, such as solar, wind, and hydropower.

Although ammonia (NH_3) is both toxic and corrosive, it is nevertheless a widely available chemical that is currently used in many industries, particularly for fertilisers. It can be transported relatively economically since it is a liquid when compressed to 10.3 bar at room temperature, or when at −33 °C at atmospheric pressure, with refrigerated tanks being the more common option [19]. Established safety working practices and health regulations exist for ammonia, related to its toxicity and corrosiveness, to ensure safe use. As a fuel, ammonia has some advantages: (i) much higher volumetric energy density compared to hydrogen; (ii) unlike hydrogen, which can be challenging to store and transport due to its low density and has exceptionally wide flammability limits, ammonia is a stable compound at room temperature with relatively narrow flammability limits; (iii) since it does not contain any carbon atom, its combustion leads to no CO_2 emission. Ammonia can also act as a hydrogen energy carrier, given that it has the highest gravimetric and volumetric hydrogen density of any H_2 compound [16]. In particular, when comparing it to the volumetric energy density of both liquid hydrogen (9.1MJ/l) and compressed ammonia (5.6 MJ/L at 70 MPa), that of liquid ammonia is higher at 15.6 MJ/l which is an important consideration for the bunkering of a marine fuel. This value is, however, only just over one third that of most hydrocarbons.

However, ammonia presents several challenges when used in internal combustion engines (ICE), originating from its particular thermophysical characteristics. Firstly, ammonia has a very low flame speed (as a result of its slow chemical kinetics [12]), especially when compared against low carbon fuels such as hydrogen, methanol and methane: 0.07 m/s for NH_3, 0.36 m/s for CH_3OH, 3.51 m/s for H_2 and

0.38 m/s for CH_4 at 300 K, 100 kPa [16]. Secondly, ammonia has a particularly high auto-ignition temperature: 924K at 100 kPa (compared to 503 K and 573 K for diesel and gasoline, respectively) [23]. These two characteristics, combined with ammonia's narrow flammability range, renders pure ammonia challenging as fuel in an ICE [19,24]. Furthermore, its enthalpy of vaporisation at 1 bar is 1371 kJ/kg, i.e., four times higher than that of diesel (317 kJ/kg) [25].

Ammonia's excessively high autoignition temperature poses a major challenge for its usage as single fuel in compression ignition (CI) engines, where the ignition of the charge relies on the fact that the in-cylinder thermodynamic conditions upon the injection of the fuel will be appropriate to initiate ignition. Of course, these conditions depend on factors like the engine's compression ratio, the intake pressure and temperature, but research has shown that pure ammonia is unsuitable for use in conventional CI engines that traditionally operate over a range of compression ratios between 15 and 22 [12,19,26,27]. One way to address this major challenge is to use ammonia in a so-called 'dual-fuel' configuration where ignition is achieved by the injection of a more reactive fuel, typically diesel. Reiter and Kong conducted two studies using ammonia and diesel with varying the mixture ratio. A 95%/5% ammonia to diesel ratio (on an energy basis) resulted in successful engine operation but was accompanied by high levels of NOx emissions [28]. Mixtures of 60%/40% and 40%/60% showed that when the ammonia ratio increased, so did NOx emissions [29]. Similarly, Gross and Kong [30] and Ryu et al. [31] experimented with the use of ammonia with dimethyl ether (DME) as the ignition source. The results showed that as NH_3 was added, NOx emissions increased, and engine performance decreased, as ammonia addition had a detrimental effect on the combustion of the mixture, thereby limiting the operational range of the engine.

To tackle ammonia's aforementioned deficiencies, the mixing of ammonia with hydrogen has been proposed [32–35]. Although Hydrogen has but a marginally lower auto-ignition temperature (844 K at 1 atm), it has a uniquely faster flame speed (3.51 m/s) and some of the widest flammability limits of any fuel. In addition, hydrogen has the potential to be produced on-site through ammonia cracking, thereby potentially eliminating the need for extensive hydrogen bunkering tanks and containment system dedicated to hydrogen storage [18]. The hydrogen generation system uses a cracking reactor that houses a ruthenium-based catalyst, which has a separate heating unit for cold starts and an exhaust gas recirculation (EGR) unit to add heat to the reaction process during engine operation [36]. The technology has advanced to the use of hollow fibre converters, combining ruthenium and carbon xerogel on a packed reactor bed, allowing for a smaller, cheaper, yet more efficient form of hydrogen cracking [37]. Given that space is generally available on most maritime vessels, hydrogen cracking, with continuous technological advancements, appears to be a potentially attractive approach to allow for hydrogen addition. By adding hydrogen, an ICE can operate without large modifications [24,27,38–40]. Thus use of ammonia/hydrogen blends in CI engines has recently received some notable traction in the research community.

Although hydrogen has lower autoignition temperature than ammonia, it is not possible to ignite such blends directly in conventional CI engines; two strategies have been proposed to address this issue. The first one is to preheat the air (or the charge) before entering the engine cylinder. Pochet et al. [41] have used ammonia/hydrogen blends in a homogeneous charge compression ignition (HCCI) engine (displacement volume of 0.499 l, engine speed of 1,500 rpm, compression ratio 16:1) in order to investigate the production of NOx emissions as a function of the ammonia share. They managed to achieve stable combustion with up to 70%vol. ammonia share using 1.5 bar intake pressure and 473 K intake temperature, but highlighted the need to minimise the intake temperature in order to maximise power and the use of exhaust gas recirculation (EGR) to tackle the NOx emissions. The same group later used a different HCCI engine with a compression ratio of 22:1 and an intake temperature ranging from

323 to 513 K (displacement volume of 0.436 l, engine speed of 1,500 rpm) for a wide variety of ammonia/hydrogen fuel blends (NH_3: 0%–95% /vol) [42]. Their work corroborated further the need for EGR to reduce effectively NOx emissions. However, the use of EGR came with the caveat of increased N_2O emissions, which is a strong 'greenhouse gas', and the authors concluded that the combustion temperature needs to be maintained substantially above 1,400 K to ensure low levels of N_2O production. Wang et al. [43] used a conventional CI engine with enhanced air preheating (551K) to investigate the optimal (in terms of power and emissions) compression ratio (from 13.5:1 to 16.5:1) and direct injection strategy for different ammonia/hydrogen blends. Their work reported that retarding the injection timing leads to power reduction, NOx decrease and N_2O increase, while the increase of the compression ratio can lead to improvement of power, accompanied by the progressive increase of both NOx and N_2O emissions. The same group used a numerical approach to investigate the effect of different inlet temperatures (476K–551K) and different ammonia/hydrogen blends on the engine's power and emissions [44]. The authors reported that in all cases the increase of the inlet temperature has a considerable detrimental effect on the engine power, the fuel consumption and NOx emissions.

The second strategy, as an alternative to the preheating of the incoming air, is the use of pilot fuel injection, the fuel being chosen to be more reactive than either ammonia or hydrogen in the sense of possessing a much lower autoignition temperature, that can thereby initiate the ignition of the surrounding ammonia and hydrogen mixture with air. This is sometimes called a 'dual fuel' strategy in the industry. Often, diesel is chosen to be the pilot fuel. Wang et al. [45] investigated numerically the effect of different ammonia/hydrogen blends on the engine power, combustion phasing and emissions in a 13:1 4-stroke engine. They concluded that the optimal ammonia/hydrogen blend at the examined conditions was 7:3 on a mass basis, but they highlighted that, at these conditions, NOx emissions increase significantly compared to the 0% H_2 case. The same group also investigated different injection strategies for the ammonia/hydrogen blends and diesel and identified that a combination of a suitable injection strategy and ammonia/hydrogen blend can reduce ammonia slip and N_2O production [46] substantially. Nevertheless, the authors reported that engine-out NOx emissions remain high, exceeding the emission standards of Tier III.

Although the technology of using diesel as pilot fuel to initiate in-cylinder ignition of the main, surrounding fuel-oxidant mixture is promising and convenient, it has the disadvantage of being a fossil fuel which emits GHGs and particulate matter (PM). As a result, other fuels have been investigated that can act as ignition promoters and possibly enable the use of ammonia/hydrogen blends while eliminating the challenge of high emissions. One such potential solution is hydrogen peroxide (H_2O_2). Hydrogen peroxide is already widely manufactured, distributed, and stored, with diverse applications ranging from medical use to processing and bleaching certain foods, and as a domestic cleaner and disinfectant. Its production can be on a renewable basis [47], which aligns with the targets of green combustion and production in the maritime industry. The use of hydrogen peroxide for propulsion purposes dates decades back to at least the 1940s when it was used for military applications [48]. Since then it has been continuously used in military and aerospace applications. Notwithstanding that the literature on the use of hydrogen peroxide in combustion engines is limited, recent academic research has corroborated its potential as an ignition promoter in combination with different fuels, such as diesel [49–51], hydrogen [52,53], butanol [54,55], and ammonia [56–58]. Khalil et al. [56] used zero-dimensional batch reactor simulations to investigate the chemical dynamics of ammonia/air mixtures with small doses of hydrogen peroxide and reported that reaction H_2O_2 (+M) → 2OH (+M) was the most influential in controlling the system's characteristic timescale. It was also reported that 2% of H_2O_2 addition (/vol) can decrease the ignition delay time by a factor of 30 with

a negligible increase of NO emissions. Shafiq and Tingas [57] investigated, computationally, a combination of ammonia and hydrogen peroxide blends in a 4-stroke 17:1 HCCI engine at engine speeds of 750 and 1150 rpm. Their work showed that the use of hydrogen peroxide as an ignition promoter is more advantageous than the preheating of charge as it can lead to a power increase of 65% and a 9-fold decrease in NOx emissions, demonstrating the potential of the promoter with ammonia. Dimitrova et al. [53] used a computational model of a 4-stroke 17:1 HCCI engine at engine speeds of 1000–3000 rpm and concluded that H_2/H_2O_2 blends can improve both the engine performance (IMEP, power, torque) and indicated thermal efficiency while reducing NOx emissions in an HCCI engine. Rabbani et al. [54] investigated, using tools of the computational singular perturbation (CSP) framework, the ignition dynamics of hydrogen peroxide addition to n-butanol/air mixtures in the context of zero-dimensional homogeneous simulations. It was reported that hydrogen peroxide addition tends to decrease substantially the chemical runaway (in favour of the thermal runaway) through the early production of OH radicals, thereby shortening drastically the ignition delay time. Zhou et al. [55], used a 30% vol% aqueous solution of H_2O_2 in an HCCI engine fuelled with butanol, demonstrating that commercially available peroxide concentrations could be used as a promoter, potentially world-wide and even at higher concentrations if needed in engine operations. It is noted though that H_2O_2 is readily available in the market up to about 30% (w/vol and w/w, depending on supplier specification), beyond that value its availability and convenience in use decreases significantly.

In this work, the initial condition is that of a statistically homogeneous gaseous ammonia/hydrogen blend (with the ratio between the two molecules in the blend being a parameter) present in the cylinder early in the compression stroke. Late in this stroke, an aqueous solution of hydrogen peroxide is introduced uniformly over a finite range of crank angle, simulating the process of injection, once again however as a statistically homogeneous gaseous species (in what follows, we shall refer to the process of introducing the peroxide as one of 'injection' but we remind the reader that there is no spatial variable involved in the model). This is the pilot fuel to initiate the ignition of the charge. In addition, EGR is also used in some calculations as a measure to tackle NOx and N_2O emissions. The initial condition of a low reactivity fuel (ammonia/hydrogen mixture) premixed with air at lean conditions, accompanied by EGR, followed by the introduction of a high-reactivity fuel near TDC (here, aqueous hydrogen peroxide), are features that characterise a reactivity controlled compression ignition (RCCI) engines [59]. RCCI mode can lead to high levels of fuel conversion efficiency, comparable to diesel engines, when using alternative fuels [60–62]. This is partly because RCCI mode can operate with higher compression ratios than spark ignition engines, and partly through using relatively low reaction temperatures consequent on operating lean and with EGR. Low temperature combustion contributes to low heat loss and thereby to the increase in the thermal efficiency of the engine [63]. Another benefit of the '*low temperature combustion*' is that it can lead to low levels of NOx emissions which may help to meet regulation levels for so-called criteria pollutants [64–66]. The RCCI mode also offers some flexibility in the fuels used within the combustion process [64].

Previous studies have shown the potential of using both ammonia/hydrogen and hydrogen peroxide in internal combustion engines. However, to the best of the authors knowledge, the use of hydrogen peroxide has been mostly limited to its use as an ignition promoter in the context of HCCI engines and its use as 'pilot' fuel has not been explored. As a result, the lack of research on the use of hydrogen peroxide 'pilot' to ignite a mixture of ammonia and hydrogen is a gap ripe for further work. The objective of the current work is to investigate numerically the use of aqueous hydrogen peroxide, as an ignition promoter of an ammonia/hydrogen mixture acting as the main energetic fuel in a compression ignition (CI) engine, on the engine performance, combustion phasing and emissions. The current work has

Table 1

Engine specifications.

Engine	IVECO 8360.46R
Type	4-Stroke Compression Ignition
Number of cylinders	6
Stroke	130 mm
Bore	112 mm
Displacement volume	7.8 L (1.3 L per cylinder)
Compression ratio	17.6:1
Maximum power	166 kW @ 2050 RPM
Maximum torque	965 Nm @ 1250 RPM

some substantial differences compared to the earlier works of Dimitrova et al. [53] and Shafiq and Tingas [57], namely: (i) the introduction of hydrogen peroxide in liquid form early in the power stroke, instead of its use in fumigated form at the start of the compression cycle; (ii) the temporal stratification of the mixture instead of a fully homogeneous mixture; (iii) the use of an ammonia/hydrogen blend as main fuel instead of either pure ammonia or pure hydrogen. To accomplish the goal for this zero-carbon and zero-sulphur fuel technology, a stochastic reactor model will be employed. We investigate different strategies for the introduction of the aqueous peroxide, variable amounts of H_2 share in the ammonia/hydrogen blends, and different EGR rates in a medium-speed 4-stroke CI engine. The results identify the potential of this technology, thereby to provide a baseline for future analyses of this fuel combination, which can be investigated in either higher-fidelity simulations or engine experiments.

2. Methods

The engine that is studied is a boosted, four-stroke, CI, IVECO design with specifications for boosted, diesel fuel operation summarised in Table 1. The engine has also been previously used in dual-fuel mode with natural gas and diesel as the low and high reactivity fuels, respectively [67].

In the current work, a commercially available stochastic reactor model (SRM) (SRM Engine Suite from CMCL Innovations [68]) has been employed which has been successfully used in other engine studies, e.g., [69–72]. A detailed description of the mathematical formulation of the model can be found in Ref. [73]. The numerical model solves a joint scalar Probability Density Function (PDF) transport equation [74] using a stochastic numerical method. The model assumes that the contents of the reactor are statistically homogeneous which means that the probability of any property (e.g. temperature or species concentration) to take a particular value is independent of the spatial position within the reactor [73]. The model resolves, as a function of time, the joint PDF that describes the state of the reactor, but not as a function of space. This results in a computationally efficient method that maintains a detailed treatment of the chemistry, and in particular that of the autoignition process, which is a transient kinetic phenomenon. The trade-off is the lack of spatial information for reduced computational time [73].

The model calculates the evolution of the N chemical species' mass fractions ($Y_i, i = 1...N$), temperature (T) and the NP stochastic particle matter state–space properties ($P_i = 1...NP$) as a function of time, which can all be represented by vector $\boldsymbol{\psi}$:

$$\boldsymbol{\psi} = (\psi_1, \ldots, \psi_N, \psi_T, \psi_{N+2}, \ldots, \psi_{NP}) = (Y_1, \ldots, Y_N, T, P_1, \ldots, P_{NP}) \quad (1)$$

The distribution of $\boldsymbol{\psi}$ is given by the PDF f, while mean quantities can be calculated by Eq. (2):

$$\langle \psi_j(t) \rangle = \int \psi_j f(\boldsymbol{\psi}; t) \, d\psi \quad (2)$$

In the problem under study, the PDF is transformed into a mass density function (MDF) $\boldsymbol{F}$ to take into account the variation in the mass:

$$\boldsymbol{F}(\boldsymbol{\psi}; t) = \rho(\boldsymbol{\psi}) f(\boldsymbol{\psi}; t) \quad (3)$$

where ρ is the mass density. The multi-dimensional MDF is then solved using a Monte Carlo particle method, where an ensemble of NP stochastic particles makes up a statistical representation of the MDF, approximated by Eq. (4):

$$f(\boldsymbol{\psi}; t) \approx \frac{1}{NP} \sum_{i=1}^{NP} \delta \left(\psi - \psi^{(i)}(t) \right) \qquad i = 1, \ldots, NP. \quad (4)$$

where δ is the Dirac delta function. A number of different statistical weighting methods can be then used to assign the statistical weights of the stochastic particles that are used to describe the distribution of the dependent variables (composition and temperature) in the engine cylinder. The employed statistical method (in the current work a quadratic weighting method was used) caters also for the distribution of the stochastic particles within the reactor volume. The time evolution of $\boldsymbol{F}$ is described by Eq. (5):

$$\frac{\partial}{\partial t} \boldsymbol{F}(\boldsymbol{\psi}; t) = \mathcal{O}_{chem} + \mathcal{O}_{turb} + \mathcal{O}_{piston} + \mathcal{O}_{conv} + \mathcal{O}_{inj} \quad (5)$$

where $\mathcal{O}_{chem}, \mathcal{O}_{turb}, \mathcal{O}_{piston}, \mathcal{O}_{conv}, \mathcal{O}_{inj}$, denote the processes associated with the chemical source term, turbulent mixing, piston movement, convective heat transfer and fuel injection, respectively.

The contribution of the chemical source term to Eq. (5) is represented by Eq. (6):

$$\mathcal{O}_{chem}(\boldsymbol{\psi}; \boldsymbol{F}(\boldsymbol{\psi}; t)) = \sum_{j=1}^{N+1} \frac{\partial}{\partial \psi_j} G_j(\boldsymbol{\psi}) \boldsymbol{F}(\boldsymbol{\psi}; t) \quad (6)$$

where the $G_j(\boldsymbol{\psi})$ functions represent species and temperature source terms, in units as defined in the $\boldsymbol{\psi}$ vector (i.e., mass fractions and Kelvin per second) and have the form:

$$G_j(\boldsymbol{\psi}) = \begin{cases} \dfrac{w_j M_j}{\rho}, & j = 1, \ldots, N \\ -\dfrac{1}{c_v \rho} \sum_{k=1}^{N} u_k M_k w_k - \dfrac{\rho}{c_v m} \dfrac{dV}{dt}, & j = T \end{cases} \quad (7)$$

where w_j is the production rate of species j, M_j is the molecular mass of species j, m is the total mass of the mixture, c_v is the specific heat capacity at constant volume, u_k the specific internal energy of the species j, V the cylinder volume. The convective heat transfer term $\mathcal{O}_{conv}$ is modelled by Eq. (8):

$$\mathcal{O}_{conv} = -\frac{\partial}{\partial \psi_{N+1}} U(\psi_{N+1}) F(\boldsymbol{\psi}; t) \quad (8)$$

where $U(\psi_{N+1})$ the function that determines the amount of heat that is transferred between the cylinder charge and the cylinder walls during each time step and is modelled by Eq. (9):

$$U(\psi_{N+1}) = -\frac{h_g A}{c_v m}(T - T_w) \quad (9)$$

where h_g is the heat transfer coefficient calculated from the Woschni heat transfer correlation, A is the available heat transfer area, and T_w the wall temperature. It is noted that the convective heat transfer term in Eq. (8) is modelled by a finite difference scheme:

$$\frac{\partial}{\partial \psi_{N+1}} U(\psi_{N+1}) F(\boldsymbol{\psi}; t)$$
$$= \frac{1}{h} [U(\psi_{N+1} + h) F(\psi_1, \ldots, \psi_N, \psi_{N+1} + h; t) - U(\psi_{N+1}) F(\boldsymbol{\psi}; t)] \quad (10)$$

where h determines the amplitude of the temperature fluctuation. Instead of a deterministic process, in which every particle transfers heat with the walls, a stochastic jump process is used, thereby producing inhomogeneities in the temperature distribution [73]. The piston movement $\mathcal{O}_{piston}$ in Eq. (5) is modelled by Eq. (11):

$$\mathcal{O}_{piston} = -\frac{1}{V(t)} \frac{dV}{dt} F(\boldsymbol{\psi}; t)) \quad (11)$$

where $V(t)$ is the volume of the engine cylinder at time t. The fuel injection term $\mathcal{O}_{inj}$ in Eq. (5) is modelled by Eq. (12):

$$\mathcal{O}_{inj} = \frac{F_f(\boldsymbol{\psi}; t)}{\tau_f} \quad (12)$$

where $F_f(\psi;t)$ is the mass density function of the fuel and τ_f is the injection time. In the current work a PDF-based injection model is adopted where evaporation is distributed according to a user-defined PDF profile that is described next. The turbulent mixing term $\mathcal{O}_{turb}$ in Eq. (5) is calculated using the Hybrid Mixing Model (HMM), which combines the coalescence-dispersion (Curl) mixing model [75] before the first injection event, and the localness mixing model (LMM) thereafter. This approach ensures the computational efficiency of the Curl model with the benefits of the LMM model where the simulation is expected to be sensitive to the turbulent mixing. The coalescence-dispersion mixing model provides a phenomenological model of turbulent mixing: pairs of particles are randomly selected and then get fully mixed, such that each particle assumes the mean composition of the particle pair [73]. The LMM works by identifying neighbouring particles, based on their proximity in composition space. The model is constrained such that mixing can occur between neighbours only. The particles are designated as being in either a mixing or a non-mixing state, and are moved between states depending on a non-dimensional age property [73]. The PDF injection model applied the Sauter Mean Diameter (SMD) on a global level and allows evaporation to be distributed according to a user-specified PDF profile. At each timestep, the mass of liquid fuel to be injected is computed, followed by the calculation of the total evaporated mass. The total evaporated mass m_f is then distributed to the stochastic particles throughout the combustion chamber based on Eq. (13):

$$\Delta m_f^{(i)} = F^{(i)} m^{(i)}, \qquad for \quad i = 1, \ldots, NP \tag{13}$$

where $m^{(i)}$ the mass of the ith particle and the function $F^{(i)}$ is given by Eq. (14):

$$F^{(i)} = e^{-\alpha\left(\frac{m^{(i)}}{\sum_{i=1}^{NP} m^{(i)}}\right)^2} \tag{14}$$

where α is a user-specified parameter which essentially controls the distribution of the evaporated fuel (in the current study the default value of 50 was used). The distribution of the evaporated mass took also into account the arrangement of the injector in the engine cylinder because particles closer to the injector received more evaporated mass than others farther away. In this way, although the model does not solve in space Eq. (5), it does take into account aspects that arise from the spatial arrangement and layout of the engine cylinder and the injector. For more details on the models employed by SRM, the reader is referred to Ref. [73]. The parameters used in the SRM are summarised in Table 2.

The SRM software accounts for the effects of inhomogeneities in the combustion chamber, providing results that are more precise than those obtained from other zero-dimensional models [76]. The stochastic particles can interact with the cylinder walls and other particles during turbulent mixing, mimicking the behaviour of fluid particles [77]. To compute the combustion parameters, the SRM software uses detailed chemical kinetics. The NH_3/H_2 chemical mechanism applied consists of 38 species and 263 reactions, which has been validated in combustion chemistry studies [78] and was used to model the fuel in the present study.

To determine the power generated per cylinder, Eq. (15) is used:

$$P_i = \frac{W_{in} N}{nR} \tag{15}$$

where P_i represents the indicated power, W_{in} represents the indicated work, N is the number of crank revolutions per second, and nR is the number of crank revolutions for each power stroke per cylinder. The indicated torque can then be determined by Eq. (16)

$$T = \frac{P_i}{2\pi N} \tag{16}$$

while the indicated thermal efficiency ϵ_{th} is defined as follows:

$$\epsilon_{th} = \frac{1}{sfc \times Q_{HV}} \tag{17}$$

Table 2
Parameters used in the stochastic reactor model.

Initial in-cylinder fuel mass	105 mg
Initial in-cylinder pressure	1.3 bar
Initial in-cylinder temperature	390 K
Simulation start	−180 CAD aTDC
Simulation end	180 CAD aTDC
Step size	0.1 CAD
Solver relative tolerance	1.0E−05
Solver absolute tolerance	1.0E−10
Sauter Mean Diameter	10 μm
Nozzle number	6
Nozzle diameter	0.16 mm
Heat transfer model	Stochastic
Heat transfer correlation	Woschni
Woschni C1 parameter	2.28
Woschni C2 parameter	0.02
Stochastic heat transfer constant	2000
Piston wall temperature	550 K
Cylinder head surface area ratio	1.2
Turbulence timescale	0.002 s
Turbulence timescale during injection	0.001 s
Turbulence timescale mode	Empirical k-ϵ model
Turbulence mixing mode	Hybrid
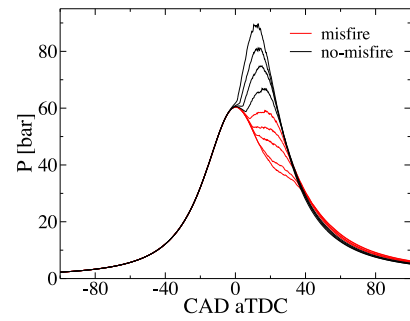
Fig. 1. Examples of cases considered as misfires in the current study compared to healthy engine cycles.

where sfc the specific fuel consumption and Q_{HV} the lower heating value of the fuel.

Misfire is a term more commonly used in spark ignition (SI) engines to denote poor combustion, or even its absence. This term will be used in the current work as well to denote a weaker than expected heat release rate – readily detected in the pressure trace – following the direct injection of the pilot fuel. A few examples of cases considered as misfires in the current study compared to healthy engine cycles are displayed in Fig. 1.

In this study, the engine parameters were set according to Table 1 in combination with the parameters in Table 2. The NH_3/H_2 blend was maintained constant at 0.8/0.2 per fuel mole fraction for all simulations, except for the cases that the hydrogen share was the variable being tested. The compression ratio was maintained at 17.6:1 and the stroke and bore were set to 130 and 112 mm, respectively. The initial in-cylinder pressure and temperature were set to 1.3 bar and 390K, respectively, representing mild boost and efficient intercooling which also avoided the condensation of water vapour (note that we have not attempted to match the details of the boosting of the IVECO engine). These values are deemed suitable based on previous studies that used ammonia and hydrogen with diesel as pilot fuel at temperatures over 400K and up to 1.5 bar [43–45]. The simulations were conducted from −180 crank angle degrees after top dead centre (CAD aTDC) to +180 CAD aTDC. Unless otherwise stated, the intake NH_3/H_2 fuel quantity was set to 105 mg, resulting in a fuel consumption rate of 7.875 kg/h at 1250 RPM, with the mass fractions of NH_3/H_2 0.9713/0.0287 and their respective mole fractions being 0.8/02. The corresponding global equivalence ratio (φ) varied between 0.54 with no EGR to 1.07 with

30% EGR, indicating a progression to fuel richer mixtures. It is noted that the EGR composition (only external EGR is considered) was maintained constant for all cases as follows: N_2 with 76%, H_2O with 16% and O_2 with 8% on a mass basis. It is also highlighted that H_2O_2 is assumed to be in aqueous form with concentrations equal or less than 30% /vol. This an important point because H_2O_2 is readily available in the market up to only 30% /vol. Above such concentrations, safety considerations become increasingly stringent.

Ammonia has a mass energy density of 18.8 MJ/kg and hydrogen has a mass energy density of 120.7 MJ/kg. When the two are mixed at NH_3/H_2 0.8/02 per mole fraction, the resulting energy mass density is 21.7 MJ/kg, which is substantially higher than the energy density of aqueous hydrogen peroxide at concentrations of either 30% /vol (1.40 MJ/kg) or 10% /vol (0.54 MJ/kg). Injection parameters were adjusted with the understanding that the injected hydrogen peroxide solution should occupy less than 10% of the volume of the ammonia in the combustion chamber when in the liquid phase. The motivation for this approach is that, in a dual fuel system, it is desired to minimise the dependence on the second fuel and hence limit as much as possible the size of the respective fuel tank. The mass of 105mg of ammonia/hydrogen fuel per cycle contains 102 mg of ammonia. This ammonia content corresponds to the vapourisation of a volume of 0.14 ml. In most simulations, the amount of the directly injected aqueous H_2O_2 (H_2O_2 10% /vol) was 4 mg which corresponds to 0.0038 ml (0.0034 ml in the case of 30% /vol H_2O_2), representing as little as 2.7% of the NH_3 fuel volume per cycle (2.4% in the case of 30% /vol H_2O_2). It is noted that in energy terms, the amount of 4 mg of aqueous H_2O_2 (H_2O_2 10% /vol) corresponds to an even smaller proportion, 0.09%, of the energy in the 105mg of the initial fuel NH_3/H_2 (0.8/0.2 per mole fraction); 0.0022 kJ for aqueous H_2O_2 and 2.28 kJ for NH_3/H_2.

The evaluation of the performance of the SRM against engine experiments is summarised in Table 1 from the previous works by Cordiner et al. [67] and Maurya and Mishra [79], which described the experimental setup and test conditions using natural gas and a diesel pilot. In particular, Maurya and Mishra [79] performed engine model validation against the engine experiments reported in Cordiner et al. [67] at two different mixtures of natural gas/diesel: 70/30 and 90/10, on an energy basis. Their validation included the pressure history and the heat release rate profile, showcasing accuracy similar to or, in certain cases, better than the respective 3D CFD simulations. Such accuracy was comparable to others reported in the literature, e.g., Pasternak et al. [72] who validated a different (from the one used herein) CI engine model (in view of pressure history and heat release rate) using diesel as sole fuel, while more recently, Saxena and Maurya [69] validated their HCCI engine model against engine experiments using syngas/hydrogen blends (in view of the pressure histories, in wide range of operational conditions). A test was performed to identify the minimum for accuracy number of particles to be used in the SRM. For this test the conditions summarised in Tables 1 and 2 were employed and the injected fuel was 16 mg of aqueous H_2O_2 with a concentration of H_2O_2 at 10% /vol, the injection timing being 0 CAD aTDC, the injection duration being 2 CAD and without the use of any EGR. By increasing the number of particles progressively from 50 up to 200, the analysis revealed that only minor differences were manifested in the results when the number of particles increases above 100. The results of this analysis are displayed in Fig. 2 where it is confirmed that, above 100 particles, the results on IMEP, NOx, maximum pressure and the maximum pressure rate of change all level off, while the differences in the pressure history become negligibly small.

3. Results and discussion

A campaign of numerical simulations has been undertaken in order to explore the different aspects of the proposed technology. The campaign was split into 5 sections based on the variable that was modified each time. Firstly, the focus was on the effect of the hydrogen

share in the initial NH_3/H_2 mixture. That analysis was conducted for three different masses of directly injected H_2O_2/H_2O mixtures. Next, the effect of the directly injected mass was explored in more detail while keeping fixed all other parameters. This analysis was performed for three different cases of start of injection (SOI). Following that, an extensive campaign was undertaken for a wide range of SOIs for three different cases of injection durations. To mitigate some of the undesired effects of ammonia combustion such as NOx emissions, the use of EGR was then investigated extensively. This investigation was conducted for three different cases of H_2O_2 share in the aqueous H_2O_2, from 10 up to 30% /vol. The three cases of H_2O_2 share were selected to include only H_2O_2/H_2O mixtures that are readily available in the market. The last part was focused on the effects of load variation, which was achieved by adjusting the mass of the injected NH_3/H_2 mixture.

3.1. Hydrogen share analysis

All simulations under this heading have been initialised with a blend of ammonia and hydrogen, with a total mass of 105 mg and with a ratio between the two fuels as a parameter. Table 3 lists the variation of the H_2 and NH_3 energy shares as a function of the NH_3/H_2 composition. This approach, along with the inhomogeneities considered through the stochastic features of the model (see Section 2 for more details), aim to simulate the in-cylinder conditions of an RCCI engine where the low reactivity fuel is spatially homogeneous early in the compression stroke with the high reactivity fuel injected later and close to top dead centre of compression, thereby leading to some control of the timing of the start of combustion – through autoignition – in the more reactive fuel, accompanied by a degree of fuel stratification and, ultimately, to staged heat release. Since ammonia is substantially less reactive than hydrogen, any addition of hydrogen should accelerate (to some degree) the combustion process in the engine cylinder. Initially, the parameters of the directly injected H_2O_2/H_2O fuel mixture, i.e., the total mass, the concentration of H_2O_2, the injection timing and injection duration were fixed at 4 mg, 10% /vol, SOI −2 CAD aTDC, 1 CAD, respectively. The analysis revealed that under these conditions (including the initial temperature and pressure of the main charge at BDC chosen for these simulations) the blend had to contain more than 15% /vol of H_2 in the NH_3/H_2 initial mixture to enable the combustion of the mixture. As Fig. 3 shows, when H_2 is 10% /vol in the NH_3/H_2 blend, no combustion occurs while when this is increased to 20% the mixture combusts, as indicated by the increase of the temperature and the heat release rate. However, the combustion at 20% /vol of H_2 occurs late during the expansion stroke (CAD50 = 15.12 CAD aTDC) and it is relatively slow (CAD90-CAD10 = 19.6 CAD). When the hydrogen share increases further to 30% /vol in the NH_3/H_2 blend, strong combustion occurs which is manifested not only in the rapid pressure increase but also in the CAD50 and CAD90-CAD10 values which both decrease drastically (6.8 CAD aTDC and 7.2 CAD, respectively). In fact, the pressure rise rate reaches a maximum value of 87.7 bar/ms (11.7 bar/CAD) which is well beyond the typical limit for conventional CI engines (approximately 50 bar/ms or 6.7 bar/CAD). Further increase of H_2 to 40% /vol in the initial fuel mixture makes the aforementioned outcomes more pronounced, i.e., the pressure rise rate increases further to 135.4 bar/ms, combustion occurs even earlier (CAD50 = 4.6 CAD aTDC) and more rapidly (CAD90-CAD10 = 5.4 CAD). All these results are consistent with earlier works which have reported that when the hydrogen share becomes higher than 30%, the risk for engine knock rises significantly (e.g.,[44]).

The effect of the increase of the hydrogen share in the NH_3/H_2 blend was further investigated by varying also the mass of the directly injected H_2O_2/H_2O pilot fuel. Similar to the preceding investigation, the concentration of H_2O_2, the SOI and injection duration were fixed at 10% /vol, −2 CAD aTDC, 1 CAD, respectively. Fig. 4 summarises the results of this numerical campaign. Firstly, it can be observed that
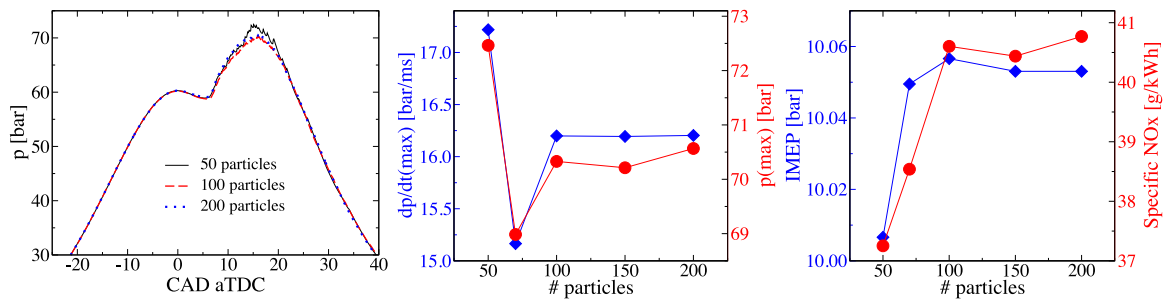
Fig. 2. Variation of the pressure history, the maximum pressure, the maximum pressure rate of change, IMEP and specific NOx for the different cases of number of particles (from 50 up to 200). The engine simulations were performed using 16 mg of injected H_2O_2/H_2O fuel mixture with a concentration of H_2O_2 at 10% vol%, the initial NH_3/H_2 mixture was 105 mg with the H_2 share being 20% vol%, the injection timing of 0 CAD aTDC, injection duration of 2 CAD and without the use of any EGR.

Table 3
The variation of the energy shares of H_2 and NH_3 for various NH_3/H_2 fuel blends.

% vol H_2	% vol NH_3	Total Fuel Energy [kJ]	% Energy H_2 share	% Energy NH_3 share
0	100	1.97	0	1.97
10	90	2.11	7.8	92.2
20	80	2.28	15.9	84.1
30	70	2.49	24.5	75.5
40	60	2.75	33.5	66.5
50	50	3.1	43.1	56.9
100	0	12.6	100	0

(a) (b) (c)
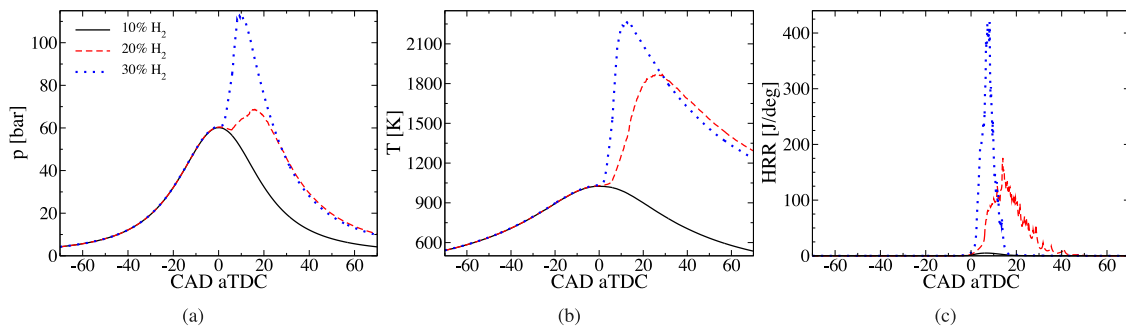
Fig. 3. Variation with crank angle of: pressure (a), temperature (b) and heat release rate (c) for 4 cases of H_2 mix with NH_3, (10%, 20%, 30% /vol). In all cases, 4 mg of H_2O_2/H_2O (10:90 /vol) is directly injected at −2 CAD aTDC with an injection duration of 1 CAD.

(a) (b) (c) (d)

(e) (f) (g) (h)
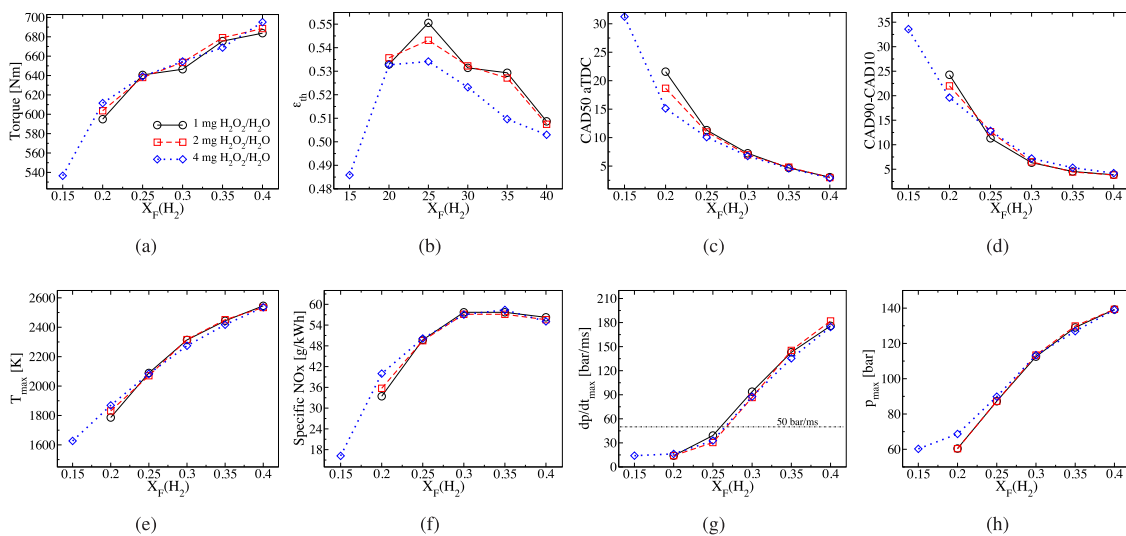
Fig. 4. The change in torque (a), indicated thermal efficiency (b), CAD50 (c), CAD90-CAD10 (d), maximum temperature (e), specific NOx (f), pressure rise rate (g) and maximum pressure as a function of the hydrogen mole fraction in the initial fuel H_2/NH_3 blend, for three different masses of directly injected mass of H_2O_2/H_2O (1, 2 and 4 mg) with SOI at −2 CAD aTDC and injection duration of 1 CAD.

the amount of H_2O_2/H_2O pilot fuel has little effect on the engine performance (indicated torque, indicated thermal efficiency), combustion phasing, NOx emissions, and pressure-related variables. This in practice means that the mass of H_2O_2/H_2O pilot fuel might be as little as 1 mg while achieving a medium load (~65% of the maximum rated torque of 965 Nm when using diesel fuel at 1250 rpm. Note however our earlier comments about the disparity in the levels of boost between this simulation and the operation of the engine on diesel fuel) with 20%–25% /vol H_2 share in the NH_3/H_2 blend. In fact, the increase of H_2 share from 20% to 40% leads to a 10% increase of load, from 62% to 71% of the engine's rated power when operated with diesel and at its rated boost levels. It is noted that the increase of the H_2 share from 20 to 40% corresponds to an increase of the fuel energy from 2.28 to 2.75 kJ, i.e., 20% increase. At these examined conditions the indicated thermal efficiency experiences a 3% decrease from 53% to 50%, presumably due to increased wall heat losses and poorer combustion efficiency. The increase in the load by raising the H_2 share comes with the drawback of rapid combustion; CAD50 drops drastically from 15–20 to 3 CAD aTDC, CAD90-CAD10 decreases similarly abruptly, from 20–25 to 4 CAD and, most important, the pressure rise rate increases from 15 to ~180 bar/ms. Notably, only the cases of 20% and 25% /vol of H_2 share have pressure rise rate values less than 50 bar/ms regardless of the mass of the injected H_2O_2/H_2O pilot fuel. The specific NOx emissions generally increase with the share of the H_2 and at high H_2 share they slightly decrease. In fact, NOx emissions (in terms of mass) change only marginally at high H_2 shares but since this is accompanied by a non-negligible increase of torque developed, the net effect on specific NOx emissions (which are defined on the basis of the mass of NOx per unit energy) is to decrease. The increase of NOx emissions, especially at low H_2 share, correlates well with the increase of the maximum temperature, thereby suggesting that the thermal NO route has its expected, notable effect.

In summary, the following points can be made:

- aqueous H_2O_2 can successfully ignite NH_3/H_2 charges with H_2 shares between 20 and 25% vol% with acceptable pressure rise rates;
- at the optimal conditions of 20%–25% /vol of H_2 share, CAD50 varies between 10 and 20 CAD aTDC and CAD90-CAD10 varies between 11 and 24 CAD (depending on the directly injected mass). In fact, the increase of the H_2 share has a more pronounced effect on the ignition promotion of the mixture when it is low.
- aqueous H_2O_2 can run as pilot with so low as 1 mg;
- the direct injection of 1mg of H_2O_2/H_2O in combination with 20%–25% H_2 share suffices to achieve more than 60% load of the engine's rated power when operated with diesel and at its rated boost levels.
- at the optimal conditions of 20%–25% /vol of H_2 share, NOx emissions remain above IMO's Tier III limit (roughly, one order of magnitude higher).

3.2. Injection mass and injection angle analysis

The aim of this analysis was to investigate the effect of the amount of the directly injected mass at different injection angles. As already explained, the approached proposed in the current work relies on the direct injection of H_2O_2/H_2O mixture in the engine cylinder to initiate the ignition of the charge. The concentration of H_2O_2 is kept fixed at 10% /vol and so is the H_2 share in the initial NH_3/H_2 mixture, at 20% /vol. The injection duration is constant at 1 CAD and the SOI is −4 CAD aTDC. As always, the mass of the initial NH_3/H_2 is constant at 105 mg in all cases.

The strong effect of the direct injection of H_2O_2/H_2O is displayed on Fig. 5 where it is shown that 1mg of the direct injection of H_2O_2/H_2O suffices to enable the ignition of the charge. However, the ignition in that case occurs quite late and the combustion process is quite

slow as it occurs during the power stroke when the volume of the combustion chamber expands. Hence, the case of 1 mg resembles more to a misfire. This phenomenon is due to the fact that H_2O_2 and H_2O act competitively in the combustion process: H_2O_2 tends to promote ignition by enhancing radical pool generation while H_2O tends to reduce combustion temperature. When the injected mass is sufficiently low (compared to the main fuel and the prevailing thermodynamic conditions), misfire occurs, as the ignition promoting character of H_2O_2 is weaker than the effect of H_2O. With the increase of the directly injected fuel to 4 mg the ignition process is significantly accelerated yet the maximum temperature lies well below 2,000 K. Further increase of the directly injected mass to 8 mg affects neither the combustion phasing greatly (in terms of duration or timing) nor the maximum temperature/heat release rate.

The effect of the mass of the directly injected H_2O_2/H_2O was further investigated in a more systematic manner, in view of the indicated torque, the combustion duration (in terms of CAD90-CAD10), the maximum pressure rise rate as well as specific NOx emissions and the results are presented in Fig. 6. This investigation was performed for three different cases of start of injection (SOI), 0, −4 and −8 CAD aTDC, with the injection duration maintained constant at 1 CAD. In terms of the torque developed, the increase of the injected mass has a significant effect when the mass is low, i.e., from 0.1 to 1 mg. Beyond the latter value, the combustion becomes less sensitive to the increase of the directly injected mass of the H_2O_2/H_2O mixture. This characteristic is independent of the SOI, although as the SOI is advanced generally higher torqued is produced, as expected. Finally, there are critical values in the mass of the directly injected H_2O_2/H_2O mixture beyond which any further increase has minimal effect on the increase of the torque, depending on the SOI value. At SOI 0 CAD, this critical mass is 4 mg (0.0022 kJ), while when SOI is advanced to −4 and −8 CAD aTDC, this critical mass becomes 3 (0.0016 kJ) and 2 mg (0.0011 kJ), respectively. It is also worth noting that the load achieved at these conditions (i.e., 4, 3 and 2 mg of H_2O_2/H_2O mixture with SOI at 0, −4 and −8, respectively) is 63%–65% that of the engine's rated power when operated with diesel and at its rated boost levels.

The trend in the combustion duration, as represented by CAD90-CAD10, is very similar to the one observed in the torque change: there is a rapid decrease for even a small mass of the directly injected H_2O_2/H_2O mixture, followed by a more modest decrease as the mass increases further and finally there is little further change. Unlike the indicated torque though, the SOI has a more pronounced impact on the combustion duration, decreasing with the retarding of the SOI from 0 to −8 CAD aTDC. At the critical values of the masses of the directly injected H_2O_2/H_2O mixture, i.e., 4, 3 and 2 mg (for 0, −4 and −8 CAD aTDC SOI, respectively), the combustion duration becomes 20.9, 18.7, 16.4 CAD, respectively.

In terms of the maximum pressure rise rate, advance of the SOI generally leads to higher maximum pressure rise rate values. This is expected since the advance occurs at CAD values before the TDC, i.e., during the compression stroke, when the volume decrease is accompanied by a pressure increase thereby favouring the ignition process. However, in all examined cases the pressure rise rate never exceeds the highest acceptable limit of 50 bar/ms. In fact, the highest obtained values for the various SOI strategies were all well below 50 bar/ms: 18.2, 30.5 and 40.3 bar/ms for SOI values of 0, −4 and −8, respectively. Qualitatively, the trend of the pressure rise rate as a function of the directly injected mass of the H_2O_2/H_2O mixture is similar for the different SOI cases. For low values of the H_2O_2/H_2O mixture, the pressure rise rate exhibits a negligible increase. But, as the mass of the H_2O_2/H_2O mixture rises further, the pressure rise rate increases almost linearly. Linear regression analysis reveals that as the SOI advances, the maximum pressure rise rate becomes more sensitive to the increase of the directly injected mass of H_2O_2/H_2O: the gradient of the (linear) best curve is 1.517 and 2.745 for the cases of −4 and −8, respectively (the coefficient of
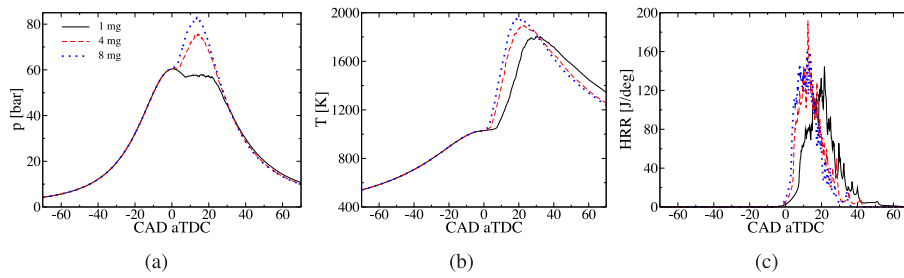
Fig. 5. The time history of pressure (a), temperature (b) and heat release rate (c) for 3 cases of directly injected mass of H_2O_2/H_2O (1, 4 and 8 mg) with the SOI fixed at −4 CAD aTDC. In all cases, the hydrogen share is kept at 20%, the injection duration is 1 CAD, the mass of the initial NH_3/H_2 mixture is 105 mg and the share of H_2O_2 in the diluted mixture is 10% /vol.
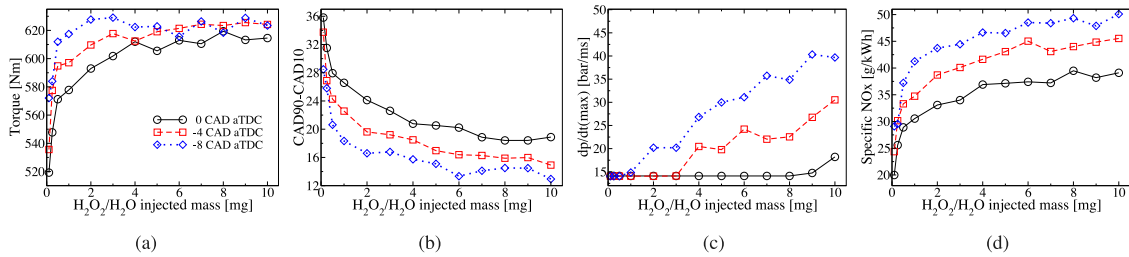
Fig. 6. The change in torque (a), CAD90-CAD10 (b), pressure rise rate (c) and specific NOx (d) as a function of the directly injected mass of H_2O_2/H_2O (from 0.1 up to 10 mg), for three different cases of SOI (0, −4 and −8 CAD aTDC). In all cases, the hydrogen share is kept at 20%, the injection duration is 1 CAD, the mass of the initial NH_3/H_2 mixture is 105 mg and the share of H_2O_2 in the diluted mixture is 10% /vol.

determination (R squared) is 0.7484 and 0.9632 for the cases of −4 and −8).

The change in specific NOx follows a pattern similar to the one described previously for the torque and combustion duration, in that for low values of the directly injected mass, an increase in the mass of the injected H_2O_2/H_2O mixture leads to a rapid change (increase) of the specific NOx: any further increase of the directly injected mass has a much smaller increase on NOx. In fact, any increase in the directly injected mass beyond the critical masses identified earlier for the different cases of SOI (4, 3 and 2 mg for SOI of 0, −4 and −8 CAD a, respectively) leads to an almost linear response to NOx emissions. This linear response is represented by gradients of 0.3338, 0.7717 and 0.8504 for SOI of 0, −4 and −8, respectively. Hence, similar to what was reported earlier about the maximum pressure rise rate, NOx emissions become more sensitive to the increase of the directly injected mass as the SOI advances. For directly injected masses of 4, 3 and 2 mg (for SOI of 0, −4 and −8, respectively) the specific NOx values are 36.9, 40.1 and 43.7 g/kWh. It is noted that these values are an order of magnitude higher than the NOx limit regulated by IMO's Tier III, which for the cases under study (engine speed of 1250 rpm) is 2.16 g/kWh.

In summary, the following conclusions can be drawn:

- 4 mg of directly injected mass of H_2O_2/H_2O suffices to achieve 65% of the rated load developed by the boosted, diesel only operation of the engine. Any further increase of the directly injected mass has negligible effect on the developed torque.
- the increase of the directly injected mass of H_2O_2/H_2O has a notable effect in decreasing the combustion duration although this effect diminishes as the directly injected mass increases.
- in all examined cases the maximum pressure rise rate was always well below the threshold of 50 bar/ms for safe engine operation. In fact, by retarding the SOI to 0 CAD aTDC, the pressure rise rate never exceeded the value of 20 bar/ms. However, by advancing the SOI the maximum pressure rise rate becomes more sensitive to the increase of the directly injected mass.
- specific NOx emissions increase with the directly injected mass of H_2O_2/H_2O and with advance of the SOI. For directly injected

masses of 4, 3 and 2 mg (for SOI of 0, −4 and −8, respectively) the specific NOx values were found to be 36.9, 40.1 and 43.7 g/kWh. These values are an order of magnitude higher than the values regulated by IMO Tier III.

3.3. Injection timing and duration analysis

Next, the analysis focused on exploring the effect of injection timing and duration on the engine performance. For this purpose, the hydrogen share in the initial NH_3/H_2 blend was kept fixed to 20% /vol, the initial NH_3/H_2 mass was 105 mg, the share of H_2O_2 in the diluted H_2O_2/H_2O mixture was 10% /vol and the mass of the directly injected mixture was held at 4 mg. The injection timing varied from −10 to +6 CAD aTDC (with a step of 2 CAD) for three different cases of injection duration, 1, 4 and 8 CAD. The results of this investigation are summarised in Fig. 7.

Firstly, it can be observed that the developed torque decreases with the delay of the SOI, regardless of the injection duration. However, this decrease is modest when the SOI is retarded from −10 to 0 CAD aTDC and, as expected, becomes substantially more pronounced when it is delayed further. In particular, torque drops from 620 Nm at SOI= −10 CAD aTDC to 612, 601 and 599 Nm at SOI=0 CAD aTDC (reductions of 8, 9 and 11 Nm) for injection durations of 1, 4 and 8 CAD, respectively. At SOI=6 CAD aTDC, torque decreases to 574, 570 and 561 Nm (further reductions of 38, 31, 38 Nm) for injection durations of 1 and 8 CAD, respectively. These results suggest that, from a load perspective, the use of H_2O_2/H_2O is to be arranged with an appropriate advance before TDC. There the load can be maintained between 60 and 65% of the engine's rated power when operated with diesel and at its rated boost levels. It is also noted that the injection duration does not appear to have a strong impact on the load developed, regardless of the SOI.

Fig. 7 also shows that the combustion duration, as represented by CAD90-CAD10, increases (more or less linearly) with retarding of the SOI for all three injection durations; the coefficient of determination (R squared) is 0.9889, 0.9897 and 0.991 for combustion durations of 1, 4 and 8 CAD, respectively. What is interesting to note here is that even with an advanced SOI (e.g., −10 CAD aTDC) and a short injection duration (say 1 CAD), the combustion duration is still to be considered
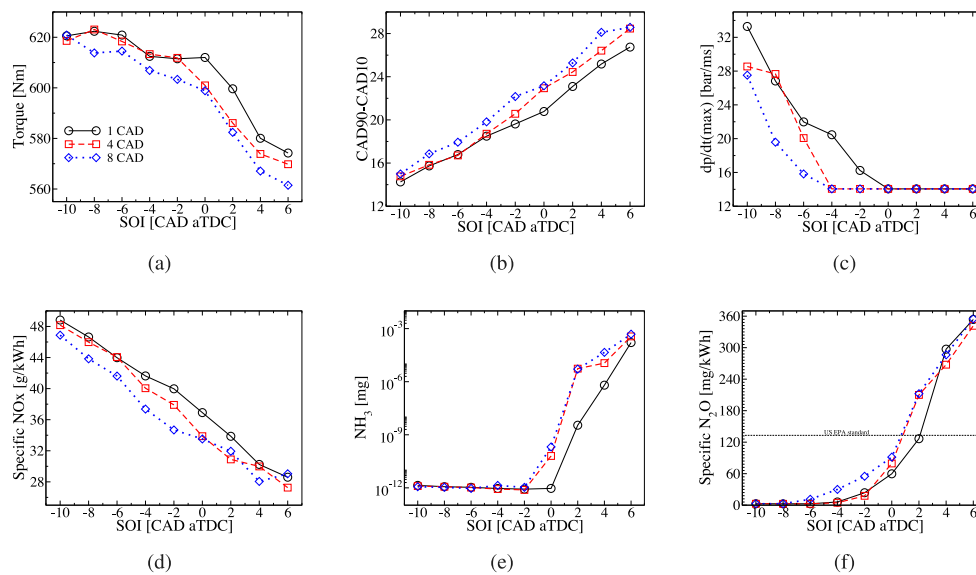
Fig. 7. The change in torque (a), CAD90-CAD10 (b), pressure rise rate (c), specific NOx (d), unburnt NH_3 (e) and N_2O production (f) as a function of the start of injection (SOI) of the H_2O_2/H_2O mixture (4 mg), for three different cases of injection duration (1, 4 and 8 CAD). In all cases, the hydrogen share is kept at 20%, the mass of the initial NH_3/H_2 is 105 mg and the share of H_2O_2 in the aqueous mixture is 10% /vol.

acceptable (14.3 CAD). This finding has also been observed in the earlier part of the study, i.e., Fig. 6. It is worth emphasising two points with respect to this pilot: (a) it is responsible for only 0.09% of the respective energy of the NH_3/H_2 fuel; (b) the standard enthalpy of vaporisation of the H_2O_2/H_2O mixture is significantly larger than conventional fuels like diesel (0.332 MJ/kg for diesel versus 2.15 MJ/kg for the H_2O_2/H_2O mixture). This implies that the evaporation of this pilot has a more intense cooling effect upon direct injection than would diesel. Similar to what was reported for the case of torque, the injection duration appears to have a relatively weak effect on the combustion duration, although this effect becomes more pronounced as the SOI is retarded.

The maximum pressure rise rate decreases drastically as the SOI is retarded from −10 to 0 CAD aTDC and levels off for any further retarding of the SOI. This is an expected outcome since the ignition is retarded with retarded SOI, thereby phasing the heat release increasingly to CAD when the chamber volume is increasing. In that sense the results displayed in Fig. 7(c) are reasonable and consistent with physical reasoning. A closer examination of the pressure histories revealed that all the cases that exhibit practically the same maximum pressure rise rate (equal to 14 bar/ms) are misfires. As a result, based on the pressure rise rate (PRR) examination, the SOI should be set between −6 and −2 CAD aTDC, as for these SOI values the PRR is kept low, while also the engine operates without any misfire. In addition, Fig. 7(c) reveals that the use of a short injection duration (1 CAD) is a more desirable schedule (although in practice it may be hard to do so with the precision required) than a longer one (say 4 or 8 CAD), as the longer injection duration requires a more advanced SOI to avoid misfire. However, the advance of the SOI is associated with higher pressure rise rates. It has to be noted though that in all examined cases, the maximum pressure rise rate was below the threshold of 50 bar/ms.

The production of specific NOx, Fig. 7(d), shows that the retarding of the SOI generally leads to lower NOx emissions. This can be explained if one considers that retarding the SOI leads not only to the increase of the combustion duration (as shown in Fig. 7(b)) but also to the retarding of the ignition process, the latter occurring in the power stroke. These two processes inevitably lead to lower temperatures, hence lower NOx emissions.

The analysis of the SOI and injection duration was extended to include examination of the unburnt NH_3 (Fig. 7(e)) as well as the production of N_2O (Fig. 7(f)). The first is important because it can lead

to the notorious ammonia slip, which is major challenge to ammonia-fired engines, while the latter is an extremely potent GHG. Regardless of the injection duration, the unburnt ammonia is negligibly low for SOI values 0 TDC aTDC or more advanced than that. Between −2 and 0 CAD aTDC (depending the injection duration) the unburnt ammonia emission increases rapidly as the SOI is retarded, but still remains at very low levels. It has to be noted, though, that the ammonia emissions for these cases are associated with engine misfire and incomplete combustion. In any case, if the SOI is advanced to −2 CAD aTDC, ammonia slip does not appear to be an issue under the current engine operation. The trend is similar for N_2O production, in that when the SOI is advanced to −2 CAD aTDC (or earlier), N_2O emissions remain below 0.006 mg, regardless of the injection duration. It is important here to highlight that N_2O emissions are not directly regulated by the IMO and there is little data on N_2O emissions from marine engines [80]. However, N_2O emissions are regulated by the U S Environmental Protection Agency (EPA) standard for medium and heavy-duty vehicles at 133 mg/kWh for the heavy-duty engine Federal Test Procedure (FTP) cycle [81]. On this basis, at least, the proposed approach would meet the US EPA's standard without the need for any after-treatment for most of the SOI values investigated here. In contrast, the standard would not be met for SOIs of 4 and 6 CAD aTDC regardless of the injection duration while at 2 CAD aTDC only the fastest injection duration would meet the regulation. It is, finally, worth noting here that the unburnt H_2 (i.e., the second component in the main fuel blend) was practically non-existent in all examined conditions (<0.00003% of the initial H_2 amount on a molar concentration basis or $<8 \times 10^{-7}$ mg).

Summarising:

- the retarding of the SOI leads, in principle, to lower torque, longer combustion duration, lower maximum pressure rise rate and lower NOx emissions. In addition, the retarding of the SOI has a notably adverse effect on the unburnt ammonia and N_2O emissions only after 0 CAD aTDC.
- the combustion duration does not have a strong impact on the examined metrics but it generally tends to decrease torque, prolong the combustion duration, increase the likelihood of misfire and reduce NOx emissions.
- to avoid misfire, the SOI needs to be advanced to −4 CAD aTDC with a short injection duration (1 CAD). Longer injection durations require earlier advance of the SOI which are in principle associated with higher pressure rise rates.

(a)   (b)
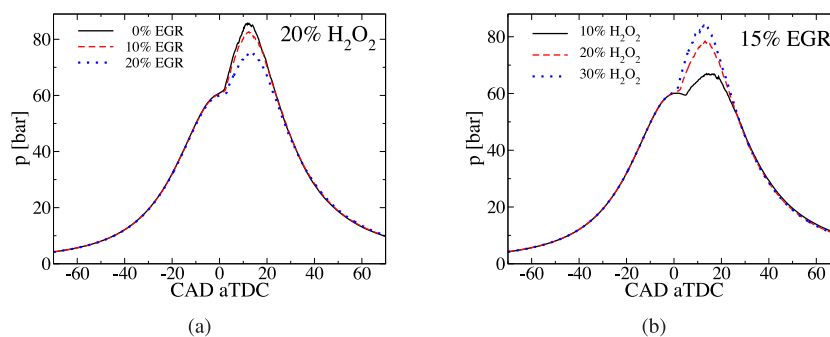
Fig. 8. The variation of pressure with CAD for: (a) three cases of different EGR rate (0, 10 and 20%) while maintaining constant H_2O_2 share at 20% /vol in the directly injected H_2O_2/H_2O mixture; (b) three cases of different H_2O_2 shares in the directly injected H_2O_2/H_2O mixture (10, 20 and 30% /vol) while maintaining constant the EGR rate at 15%. In all cases, the mass of the directly injected H_2O_2/H_2O mixture is 4 mg, the SOI is −4 CAD aTDC, the injection duration is 1 CAD, the hydrogen share is kept at 20% and the mass of the initial NH_3/H_2 mixture is 105 mg.

- with an SOI between −6 and −2 CAD aTDC and an injection duration of 1 CAD, the engine can reach a load of 63%–64% that of the engine's rated power when operated with diesel and at its rated boost levels. At these conditions, the maximum pressure rise rate is well below the threshold of 50 bar/ms (16–22 bar/ms) and the unburnt ammonia emission is negligibly small. However, NOx emissions are still an order of magnitude higher than IMO's Tier III regulation (between 39 and 44 g/kWh, compared to the threshold of 2.16 g/kWh mandated by the IMO).

- early SOI and short injection durations favour the decrease of N_2O emissions. The USA EPA's standard could easily be met (without any after-treatment) with SOIs at 0 CAD aTDC or more advanced regardless of the injection duration, while a short injection duration (1 CAD) could extend that operational limit to 2 CAD aTDC.

3.4. Exhaust gas recirculation (EGR) analysis

The next part of the analysis explores the effect of external EGR on engine performance, in combination with the variation of the H_2O_2 share in the directly injected H_2O_2/H_2O fuel. In particular, the EGR content was varied from 0 to 30% (on a mass basis of the initial air) leading to a change of the global equivalence ratio from 0.54 to 1.07 while the H_2O_2 share varies between 10 to 30% (on a volume basis). One of the known effects of EGR is the reduction of the maximum in-cylinder pressure as a result of the reduction in the available oxygen and the concurrent addition of water vapour, a triatomic molecule with consequently higher specific heat than the diatomic oxygen and nitrogen molecules. This is indeed confirmed in Fig. 8(a) where it is shown that as the EGR rate gradually increases from 0% to 20% (in the case where the H_2O_2 share is 20% /vol) the maximum pressure decreases by more than 10 bar. On the other hand, Fig. 8(b) also shows the strong effect that the increase of the H_2O_2 share has on the pressure history in the presence of external EGR (15%). It is noted that in the latter set of cases, the mass of the directly injected H_2O_2/H_2O is maintained constant at 4 mg and so is the mass of the initial NH_3/H_2 fuel (105 mg). It can be observed that doubling the H_2O_2 share from 10% to 20% on a volume basis leads to an increase of more than 11 bar while further increase to a 30% share raises the maximum pressure by another 6 bar. The ignition promotion and higher maximum pressures achieved by the increase of the H_2O_2 share are a manifestation of the radical pool enhancement achieved by H_2O_2. Radical species, namely OH and H, are directly enhanced by the increase of H_2O_2, thereby leading to an accelerated combustion process. It is noted that the increase of the H_2O_2 share from 10% to 20% and 30% vol% translates to 0.0022, 0.0040, 0.0034 kJ, respectively, which when compared against the energy content of the NH_3/H_2 fuel blend (2.28 kJ) are equivalent to 0.09%, 0.18% and 0.24%. All these results corroborate the ability of H_2O_2 to promote ignition despite its paltry energy content.

Extending the analysis to the range of 0%–30% of external EGR for all three cases of H_2O_2 share in the H_2O_2/H_2O mixture (10, 20 and 30% /vol), Fig. 9 summarises the respective results in terms of torque, combustion phasing, pressure rise rate, indicated thermal efficiency and emissions. The first observation that can be made is that, for the case of 10% H_2O_2 share, misfire occurs for EGR rates higher than 15%, while the respective threshold for 20% and 30% H_2O_2 shares is above 30% EGR rate. In other words, by increasing the H_2O_2 share in the H_2O_2/H_2O mixture, the system becomes less prone to misfire. This can be attributed to three reasons: (i) an increase of the H_2O_2 share results in an increase of the fuel's heating value (0.54/1.00/1.40 MJ/kg for the cases of 10/20/30% /vol H_2O_2, respectively); (ii) by increasing the H_2O_2 share, the radical pool essential for the ignition of the mixture is enhanced; (iii) H_2O_2 in fact can act as both fuel and oxidiser and the latter becomes particularly important when EGR is used.

The indicated torque and the indicated thermal efficiency are the two metrics least affected by the increase of EGR. The indicated torque exhibits a very small decreasing trend with EGR but this trend becomes less visible as the H_2O_2 share increases. In fact, when the H_2O_2 becomes 30% the indicated torque remains practically unaffected and hence constant with the increase of EGR. The indicated thermal efficiency exhibits a very similar response to the indicated torque, in that it remains largely insensitive to the change of the external EGR share. For a fixed EGR rate, it can also be observed that the torque increases and the indicated thermal efficiency decreases with the increase of the H_2O_2 share. The former occurs because of the higher work produced by the piston as a result of the higher pressure reached with the increase of the H_2O_2 share, as reported in Fig. 8. The latter is due to the higher heating value of the directly injected H_2O_2/H_2O mixture as a result of the increase of the H_2O_2 share.

The combustion phasing on the other hand exhibits a more pronounced response to the increase in EGR. In particular, CAD50 exhibits an almost perfectly linear increase with the increase of the EGR rate, for all three cases of H_2O_2 share. However, the dependence of CAD50 on EGR becomes less sensitive with the increase of the H_2O_2 share, as indicated by the reduction in the respective slopes. In addition, the combustion duration (as represented by CAD90-CAD10) generally increases, as expected, with the increase of EGR. The retarding of the combustion process with the increase of the external EGR is an expected outcome since EGR acts as a diluent and therefore, the more EGR in the cylinder, the slower the combustion process.

The benefits of external EGR are to be found in the pressure rise rate and NOx emissions. Fig. 9(d) shows that the maximum pressure rise rate decreases with the increase of external EGR. Hence, at 15% of EGR, the maximum pressure rise rates of 10%, 20% and 30% H_2O_2 shares are 15, 17.9 and 24.6 bar/ms, respectively. These are reductions of 32%, 29% and 10% compared to the respective cases of zero EGR share. Notice, though, that the effectiveness in the reduction in the maximum pressure rise rate becomes less pronounced as the H_2O_2
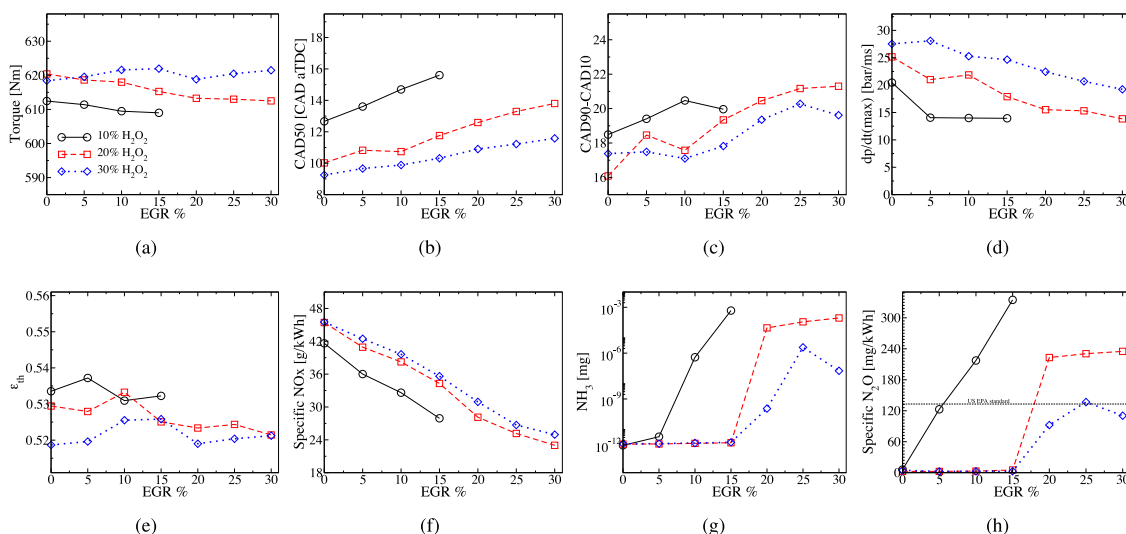
Fig. 9. The change in torque (a), CAD50 (b), CAD90-CAD10 (c), pressure rise rate (d), indicated thermal efficiency (e), specific NOx (f), unburnt NH_3 (g) and produced N_2O (h) as a function of the initial mass fraction of the external EGR, for three cases of different share of H_2O_2 in the directly injected H_2O_2/H_2O mixture (10%, 20% and 30% /vol). In all cases, the mass of the directly injected H_2O_2/H_2O mixture is 4 mg, the SOI is −4 CAD aTDC, the injection duration is 1 CAD, the hydrogen share is kept at 20% and the mass of the initial NH_3/H_2 mixture is 105 mg.

share increases. In any case, in terms of absolute values, the obtained maximum pressure rise rates are all well below the threshold of 50 bar/ms.

Similar to the maximum pressure rise rate, specific NOx emissions decrease with the increase of EGR share. This is an expected result as EGR is known to be a very effective tool for reducing NOx emissions. This is demonstrated in Fig. 9(f) where it is shown that 15% EGR can achieve 33, 24 and 22% reduction in NOx emissions compared to the zero EGR case for 10%, 20% and 30% H_2O_2 shares, respectively. It is noted, though, that even by increasing the EGR rate to 30%, specific NOx emissions still remain substantially above the acceptable limit set by the IMO (2.16 g/kWh), despite the tremendous reduction that they experience (~45%).

The analysis reveals that EGR also tends to increase the remaining NH_3 slip. However, even the largest NH_3 emissions reached at the highest EGR rates are negligibly small: 6.1 $\cdot10^{-4}$, 1.9 $\cdot10^{-4}$ and 2.4 $\cdot10^{-6}$ g/kWh, for 10%, 20% and 30% H_2O_2 shares. These values are less than 0.001% of the initial mass of NH_3 (101.98 mg), hence the degree of combustion inefficiency owing to ammonia slip is not considered a problem, at least on the basis of the calculation approach used in this work. It is also worth noting that as the H_2O_2 share increases, the amount of unburned ammonia becomes less sensitive to the increase of EGR. This definitively indicates that as the H_2O_2 share increases the system undergoes a more complete combustion, leaving progressively less unburned ammonia.

In fact, the last comment also applies for the N_2O emissions displayed in Fig. 9(h), which shows that as the H_2O_2 share increases, the engine tends to emit less N_2O across the different EGR ratios. More precisely, with 10% H_2O_2 share, N_2O emissions start increasing rapidly as soon as some EGR is used and with a 5% EGR N_2O emissions are marginally below the USA EPA's standard, while by increasing EGR further to 10% these emissions almost double, thereby exceeding, by far, the EPA's standard. On the other hand, when the H_2O_2 share increases to 20%, N_2O emissions remain extremely low and only start to increase notably as soon as EGR increases beyond 15%. Increasing the H_2O_2 share further to 30% enables the system to operate with N_2O emissions below EPA's standard for all EGR ratios examined from 0 up to 30%. Notably, both at 20 and 30% H_2O_2 shares, the N_2O emissions start increasing significantly when EGR increases beyond 15%. To understand this behaviour, we need to consider that the increase in EGR leads to the retarding of CAD50 and the extension of

the combustion duration (CAD90-CAD10), as was shown in Figs. 9(b) and 9(c), respectively. In other words, not only is combustion retarded but also its duration is longer which inevitably leads to some of the main fuel blend (NH_3/H_2) remaining unburnt for longer in the power stroke as illustrated by the right-hand ordinate of Fig. 10(a). While this happens, the thermodynamic conditions are still suitable for the activation of exothermic reactions which maintain a sufficiently high heat release rate (left hand ordinate of Fig. 10(a)) and hence high temperature (left hand ordinate of Fig. 10(b)). The sufficiently high temperature and the excess remaining main fuel blend (NH_3/H_2) lead to the generation of more radicals, particularly O radicals (right hand ordinate of Fig. 10(b)) which are the key chemical species for the production of N_2O through reaction N2 + O (+M) → N2O (+M) [82].

In summary, the investigation of the EGR ratio for different H_2O_2 shares revealed that:

- the developed torque and indicated thermal efficiency remains practically unaffected by the use of EGR, regardless of the H_2O_2 share. However, for a given EGR rate, torque increased and indicated thermal efficiency dropped with the increase of H_2O_2 share.
- CAD50 increased linearly with the EGR for all H_2O_2 shares. As expected, CAD50 was also found to decrease with the increase of the H_2O_2 share.
- the combustion duration was found to increase with the increase of the EGR rate and decrease with the H_2O_2 share.
- the use of EGR was found to be an effective measure to decrease the maximum pressure rise rate. At 15% of EGR rate, the maximum pressure rise rates of 10%, 20% and 30% H_2O_2 shares were 15, 17.9 and 24.6 bar/ms, respectively, all well below the acceptable limit of 50 bar/ms.
- specific NOx emissions also decreased substantially with EGR, yet they remained above the acceptable IMO limit (2.16 g/kWh), thereby suggesting potentially the need for some aftertreatment.
- ammonia slip was not an issue with the proposed approach because the unburned ammonia was negligibly small at all conditions.
- N_2O emissions tend to generally increase with EGR but as the H_2O_2 share increases, the system tends to emit fewer N_2O emissions across the different EGR ratios and hence it becomes easier to meet US EPA's standard.
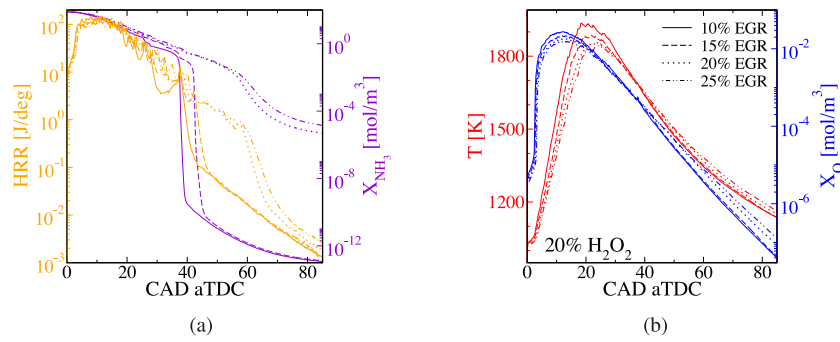
Fig. 10. The variation of heat release rate and molar concentration of NH_3 in (a), and temperature and molar concentration of O radical in (b) for four cases of different EGR rates (10, 15, 20 and 25%) while maintaining constant the H_2O_2 share at 20% /vol in the directly injected H_2O_2/H_2O mixture. In all cases, the mass of the directly injected H_2O_2/H_2O mixture is 4 mg, the SOI is −4 CAD aTDC, the injection duration is 1 CAD, the hydrogen share is kept at 20% and the mass of the initial NH_3/H_2 mixture is 105 mg.
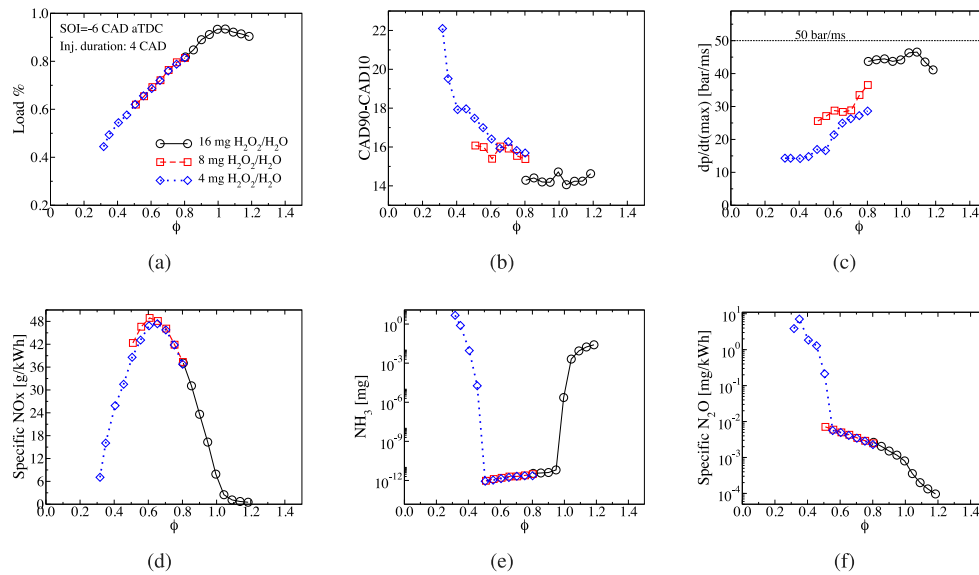
Fig. 11. The change in load (a), CAD90-CAD10 (b), pressure rise rate (c), specific NOx (d), unburnt NH_3 (e) and N_2O production (f) as a function of the initial equivalence ratio for three different cases of directly injected masses (4, 8 and 16 mg). In all cases, the hydrogen share is kept at 20%, the share of H_2O_2 in the diluted mixture is 10% /vol, the SOI is −6 CAD aTDC and the injection duration is 4 CAD.

3.5. Varying load analysis

The scope of the last section of the analysis is to explore the changes in the engine performance as a function of the load. The variation of load is achieved by adjusting the initial mass of the NH_3/H_2 mixture. Any change in that mass directly affects the in-cylinder global equivalence ratio. As a result, the equivalence ratio changes from 0.32 to 1.2 by adjusting the mass of the NH_3/H_2 mixture from 65 to 202 mg, respectively. Apart from the mass of the NH_3/H_2 mixture, all other parameters are maintained constant with the exception of the mass of the directly injected H_2O_2/H_2O mixture where three cases are considered: 4, 8 and 16 mg. Moreover, the SOI is −6 CAD aTDC, the injection duration is 4 CAD, the hydrogen share is kept at 20% and the share of H_2O_2 in the diluted mixture is 10% /vol. At this point it has to be stressed that the engine performance outcomes discussed next are achieved without applying any systematic optimisation process, because the only variables that are altered are the mass of the initial NH_3/H_2 blend and the mass of the directly injected aqueous H_2O_2. It is likely that better performance outcomes would be achieved by optimising all the pertinent engine parameters, e.g., the SOI, the injection profile, the injection duration etc.

As Fig. 11(a) shows, the load progressively increases, as expected almost linearly, from an equivalence ratio at 0.3 and peaks for stoichiometric mixtures ($\phi = 1$). An equivalence ratio of 0.3 allows a load of 44% of conventional diesel boosted operation, while at an equivalence ratio of 1.05, the load reached is 93% of the same metric. Notice that the amount of the directly injected mass has negligible effect on the engine load; for example, at $\phi = 0.8$ (148 mg initial fuel) the load is practically the same (81%) for all three different cases of directly injected mass (4, 8 and 16 mg). This is consistent with Fig. 6 where it was shown that, as soon as the directly injected mass exceeds a critical value, any further increase does not affect the developed torque. When the directly injected mass is 8 and 16 mg, the equivalence ratio (and hence load) has a relatively weak – but different – effect on the combustion duration CAD90-CAD10. However, when the directly injected mass decreases to 4 mg, the duration becomes sensitive to the change in the equivalence ratio at fuel lean conditions between 0.3 and 0.4.

The maximum pressure rise rate is found to stay below the threshold of 50 bar/ms for all investigated cases. However, it generally tends to increase with the equivalence ratio (and hence the load) from fuel lean to stoichiometric and decreases with increasing equivalence ratio in the fuel rich regime. In addition, the maximum pressure rise rate also increases with the increase of the directly injected mass, consistent with Fig. 6. It has to be noted, though, at high load conditions (equivalence ratio between 0.8 and 1.2) that the maximum pressure rise rate is relatively close to the threshold of 50 bar/ms. As a result, it would be reasonable at these conditions to make use of EGR or to optimise the injection strategy to alleviate the high pressure rise rate.

The results are equally interesting in view of emissions, i.e., NOx, unreacted NH_3 and N_2O. With regard to NOx, Fig. 11 shows that specific NOx emissions are clearly a function of the equivalence ratio: emissions peak in the neighbourhood of $\phi=0.6-0.65$ and rapidly decrease for fuel leaner or richer mixtures. This is consistent with ammonia/hydrogen combustion experiments reported in the literature which attributed the peak of NOx at such lean conditions as a result of the weak deNOx effect of ammonia [83–86]. At these equivalence ratios, the developed load is ~70% of the reference diesel operation. The specific NOx maximum value that is attained for $\phi = 0.61$ is equal to 48.9 g/kWh, i.e., 22 times higher than the Tier III regulation of 2.16 g/kWh. At highly fuel lean conditions (and low loads), i.e., $\phi = 0.3-0.35$, specific NOx drop significantly to 7–16 g/kWh, while at stoichiometric conditions where the maximum load is obtained, NOx emissions drop even further to 2.49 g/kWh, marginally above the Tier III regulation.

Any unreacted ammonia giving rise to emission has in general negligibly small values, with the peaks at the leanest and richest equivalence ratios. For example, at $\phi=0.41$ (54% load), the unreacted ammonia is 0.0092 mg which is 0.012% of the initial NH_3 mass, while at $\phi = 1.04$ (93%) the unreacted ammonia becomes 0.0021, which is 0.0012% of the initial mass of ammonia. The results indicate that ammonia slip would not be a problem for any of the conditions under investigation with the exception of highly fuel lean conditions, $\phi = 0.3$, where the unreacted ammonia can reach 7% of the initial NH_3 mass. N_2O emissions are generally maintained at very low values, well below the standard regulated by USA EPA at 133 mg/kWh. In fact, the highest value that is reached is 7 mg/kWh for $\phi=0.35$, which is nearly 20 times below the standard. Yet, it needs to be stated that N_2O emissions tend to increase as the equivalence ratio progressively decreases, thereby peaking at the fuel lean boundary of $\phi = 0.3-0.4$.

In summary:

- load variation between 44% and 93% (of the engine's rated power when operated with diesel and at its rated boost levels) can be achieved by adjusting the equivalence ratio of the initial mixture from 0.3 to 1.05, respectively. Load enhancement is almost perfectly linear with the increase in the equivalence ratio, peaking at $\phi = 0.5$.
- combustion duration is affected more by the directly injected mass than the equivalence ratio of the initial mixture. The latter has a weak impact on the combustion duration.
- the maximum pressure rise rate is a function of both the directly injected mass and the equivalence ratio of the initial NH_3/H_2 mixture, increasing with the increase of any of these two. In all cases, the maximum pressure rise rate is maintained below the threshold of 50 bar/ms.
- NOx emissions peak between $\phi = 0.6-0.65$ and rapidly decrease as the equivalence ratio increases or decreases. At high load conditions (93%) NOx emissions are marginally above the Tier III standard, at 2.49 g/kWh (compared to the standard of 2.16 g/kWh). These results, if confirmed, are unusual for ICEs which generally emit the most NOx as stoichiometric ratio is approached. While more work is needed, the results found here may allow greater operational flexibility, particularly for turbocharging.
- ammonia slip is negligible for any of the investigated conditions, with the only possibly exception at low loads (44%) and highly lean conditions ($\phi = 0.32$) where the unreacted ammonia reaches 7.4% of the initial NH_3 mass.
- N_2O emissions are negligibly small for all investigated conditions of different loads and directly injected masses.

4. Conclusions

In this study, a sophisticated and well validated stochastic reactor model has been utilised to explore the potential of using the pilot injection of hydrogen peroxide as an ignition promoter for compression ignition engines fuelled with blends of ammonia and hydrogen. Engines, fuelled with ammonia or hydrogen, are currently being investigated by the maritime industry and other heavy-duty engine sectors as promising alternatives to conventional heavy fuel oil engines, notorious for their significant pollution emissions. Despite their environmental promise, these engines still require diesel pilot injection to achieve ignition, thereby precluding them from achieving full decarbonisation.

An extensive numerical campaign was undertaken, investigating the effect of: (i) the hydrogen share in the NH_3/H_2 mixture; (ii) the amount and concentration of the directly injected mass of H_2O_2/H_2O; (iii) the SOI and the injection duration; (iv) the amount of the EGR; (v) the equivalence ratio for wide range of different engine loads. These investigations were focused on the consequences for engine load, combustion phasing and duration, maximum pressure rise rate, and emissions (NOx, NH_3, N_2O).

The analysis reported herein presents some novel findings that provide evidence for the potential feasibility of the proposed use of pilot injection of hydrogen peroxide as an ignition promoter in ammonia/hydrogen fuelled compression ignition engines. Firstly, it is shown that the required amount of aqueous hydrogen peroxide could be as low as 0.09% on an energy basis of the ammonia/hydrogen mixture at medium and high loads. If we suppose that ammonia will be stored in liquid form (and hydrogen will be produced by cracking some of that ammonia), the H_2O_2/H_2O to NH_3 share becomes only 2.6% on a volume basis (considering the densities of ammonia and H_2O_2/H_2O as 730 and 1,076 kg/m^3, respectively). Secondly, the analysis highlighted that the concentration of the hydrogen peroxide in the aqueous mixture can be as low as 10%. This is important for two reasons. Firstly, because the relatively large proportion of water associate with the peroxide solution can assist in mitigating the undesired effect of ammonia combustion, namely NOx emissions. The second reason has to do with the logistics of the H_2O_2/H_2O mixture and the fact that less concentrated solutions are more widely available in the market. The analysis also revealed that generally no excessive pressure rise rates arise that would prohibit the use of the proposed technology. The only potential exception is when the hydrogen share is more than 20% but this has been reported for other ammonia/hydrogen-based technologies, unrelated to the use of peroxide. The proposed technology nevertheless results in NOx emissions which, in many of the explored conditions, exceeded the Tier III standard, thereby necessitating the need for after-treatment. These emissions are similar to those reported in the literature [87,88], but future work on the optimisation of the injection strategy, combined with EGR, might reduce NOx emissions further. Ammonia slip was found to be negligibly small with the only exception being at extremely fuel lean conditions ($\phi = 0.3$), where the unreacted ammonia was 7% of the initial ammonia mass. Finally, N_2O emissions were generally found to be low, meeting the USA EPA's standard, although under certain conditions these increased to unacceptable levels. Further work is required with respect to this emission.

This study presents promising preliminary results. It provides grounds for further investigation into the full scope and limitations of this technology, which necessitates conducting extensive engine experiments and advanced high fidelity computational simulations. The work also highlights the necessity for more extensive analysis of the optimal configuration to achieve balance between engine performance and specific NOx levels, and outlines potential options. There is a need for more detailed examination of efficient design parameters for engine operation utilising the technology.

CRediT authorship contribution statement

Gregor Paterson: Data curation, Investigation, Software, Validation, Writing – original draft. **Efstathios-Al. Tingas:** Conceptualization, Data curation, Formal analysis, Investigation, Methodology, Project administration, Resources, Software, Supervision, Validation, Visualization, Writing – original draft, Writing – review & editing. **Yannis Hardalupas:** Formal analysis, Investigation. **Alexander M.K.P. Taylor:** Formal analysis, Investigation, Writing – original draft, Writing – review & editing.

Declaration of competing interest

The authors declare that they have no known competing financial interests or personal relationships that could have appeared to influence the work reported in this paper.

References

[1] Cullinane K, Yang J. Evaluating the costs of decarbonizing the shipping industry: A review of the literature. J Mar Sci Eng 2022;10(7). http://dx.doi.org/10.3390/jmse10070946, URL https://www.mdpi.com/2077-1312/10/7/946.

[2] Faber J, Hanayama S, Zhang S. Fourth IMO GHG study 2020 full report. International Maritime Organisation; 2020, URL https://wwwcdn.imo.org/localresources/en/OurWork/Environment/Documents/Fourth%20IMO%20GHG%20Study%202020%20-%20Full%20report%20and%20annexes.pdf.

[3] International council on clean transportation, the international maritime organization's initial greenhouse gas strategy. INTERNATIONAL COUNCIL ON CLEAN TRANSPORTATION; 2018, URL https://theicct.org/sites/default/files/publications/IMO_GHG_StrategyFInalPolicyUpdate042318.pdf.

[4] International renewable energy agency, a pathway to decarbonise the shipping sector by 2050. International renewable energy agency; 2021, URL https://theicct.org/sites/default/files/publications/IMO_GHG_StrategyFInalPolicyUpdate042318.pdf.

[5] IMO. 2023 IMO strategy on reduction of GHG emissions from ships, RESOLUTION MEPC.377(80), adopted on 7 july 2023, MEPC 80/WP.12, annex 1. 2023.

[6] The department for transport UK, Clean maritime plan. The Department For Transport UK; 2019, URL https://assets.publishing.service.gov.uk/government/uploads/system/uploads/attachment_data/file/815664/clean-maritime-plan.pdf.

[7] The department for transport UK, DfT launches UK SHORE to take maritime 'back to the future' with green investment. The Department For Transport UK; 2022, URL https://www.gov.uk/government/news/dft-launches-uk-shore-to-take-maritime-back-to-the-future-with-green-investment. [Accessed 23 December 2023].

[8] Lindstad HE, Rehn CF, Eskeland GS. Sulphur abatement globally in maritime shipping. Transp Res D 2017;57:303–13. http://dx.doi.org/10.1016/j.trd.2017.09.028, URL https://www.sciencedirect.com/science/article/pii/S1361920917304819.

[9] IMO. Nitrogen oxides (NOx) – Regulation 13. IMO; 2016, URL https://www.imo.org/en/OurWork/Environment/Pages/Nitrogen-oxides-(NOx)-%E2%80%93-Regulation-13.aspx.

[10] Ryu Y, Kim H, Cho W, Nam J. Installation and characteristics of urea-selective catalytic reduction systems for nitrogen oxide reduction in marine diesel engine. Proc Inst Mech Eng M 2017;231(3):760–7. http://dx.doi.org/10.1177/1475090217699679.

[11] Mallouppas G, Yfantis EA. Decarbonization in shipping industry: A review of research, technology development, and innovation proposals. J Mar Sci Eng 2021;9(4). http://dx.doi.org/10.3390/jmse9040415, URL https://www.mdpi.com/2077-1312/9/4/415.

[12] Tornatore C, Marchitto L, Sabia P, De Joannon M. Ammonia as green fuel in internal combustion engines: State-of-the-art and future perspectives. Front Mech Eng 2022;8. http://dx.doi.org/10.3389/fmech.2022.944201, URL https://www.frontiersin.org/articles/10.3389/fmech.2022.944201.

[13] The department for transport UK, decarbonising transport. The Department For Transport UK; 2021, URL https://assets.publishing.service.gov.uk/media/610d63ffe90e0706d92fa282/decarbonising-transport-a-better-greener-britain.pdf.

[14] The department for transport UK, UK domestic maritime decarbonisation. The Department For Transport UK; 2022, URL https://assets.publishing.service.gov.uk/media/62d7b533d3bf7f285a88f4c4/uk-domestic-maritime-decarbonisation-consultation-plotting-the-course-to-zero.pdf.

[15] Chehade G, Dincer I. Progress in green ammonia production as potential carbon-free fuel. Fuel 2021;299:120845. http://dx.doi.org/10.1016/j.fuel.2021.120845, URL https://www.sciencedirect.com/science/article/pii/S0016236121007225.

[16] Valera-Medina A, Xiao H, Owen-Jones M, David W, Bowen P. Ammonia for power. Prog Energy Combust Sci 2018;69:63–102. http://dx.doi.org/10.1016/j.pecs.2018.07.001, URL https://www.sciencedirect.com/science/article/pii/S0360128517302320.

[17] Tawalbeh M, Murtaza SZ, Al-Othman A, Alami AH, Singh K, Olabi AG. Ammonia: A versatile candidate for the use in energy storage systems. Renew Energy 2022;194:955–77. http://dx.doi.org/10.1016/j.renene.2022.06.015, URL https://www.sciencedirect.com/science/article/pii/S0960148122008473.

[18] Tingas E-A, Taylor AMKP. Hydrogen: Where it can be used, how much is needed, what it may cost. In: Tingas E-A, editor. Hydrogen for future thermal engines. Cham: Springer International Publishing; 2023, p. 3–64. http://dx.doi.org/10.1007/978-3-031-28412-0_1.

[19] Dimitriou P, Javaid R. A review of ammonia as a compression ignition engine fuel. Int J Hydrogen Energy 2020;45(11):7098–118. http://dx.doi.org/10.1016/j.ijhydene.2019.12.209, URL https://www.sciencedirect.com/science/article/pii/S0360319920300124.

[20] Cardoso JS, Silva V, Rocha RC, Hall MJ, Costa M, Eusébio D. Ammonia as an energy vector: Current and future prospects for low-carbon fuel applications in internal combustion engines. J Clean Prod 2021;296:126562. http://dx.doi.org/10.1016/j.jclepro.2021.126562, URL https://www.sciencedirect.com/science/article/pii/S0959652621007824.

[21] Gezerman AO. A critical assessment of green ammonia production and ammonia production technologies. Kemija Ind 2022. http://dx.doi.org/10.15255/KUI.2021.013.

[22] Wang C, Walsh SD, Longden T, Palmer G, Lutalo I, Dargaville R. Optimising renewable generation configurations of off-grid green ammonia production systems considering Haber–Bosch flexibility. Energy Convers Manage 2023;280:116790. http://dx.doi.org/10.1016/j.enconman.2023.116790, URL https://www.sciencedirect.com/science/article/pii/S019689042300136X.

[23] Zamfirescu C, Dincer I. Ammonia as a green fuel and hydrogen source for vehicular applications. Fuel Process Technol 2009;90(5):729–37.

[24] da Rocha RC, Costa M, Bai X-S. Chemical kinetic modelling of ammonia/hydrogen/air ignition, premixed flame propagation and NO emission. Fuel 2019;246:24–33. http://dx.doi.org/10.1016/j.fuel.2019.02.102, URL https://www.sciencedirect.com/science/article/pii/S0016236119303163.

[25] Linstrom P, Mallard W, et al. NIST standard reference database number 69. In: NIST chemistry webbook. National Institute of Standards and Technology Gaithersburg MD; 2005, p. 20899.

[26] Kurien C, Mittal M. Review on the production and utilization of green ammonia as an alternate fuel in dual-fuel compression ignition engines. Energy Convers Manage 2022;251:114990. http://dx.doi.org/10.1016/j.enconman.2021.114990, URL https://www.sciencedirect.com/science/article/pii/S0196890421011663.

[27] Chiong M-C, Chong CT, Ng J-H, Mashruk S, Chong WWF, Samiran NA, et al. Advancements of combustion technologies in the ammonia-fuelled engines. Energy Convers Manage 2021;244:114460. http://dx.doi.org/10.1016/j.enconman.2021.114460, URL https://www.sciencedirect.com/science/article/pii/S0196890421006361.

[28] Reiter AJ, Kong S-C. Diesel Engine Operation Using Ammonia as a Carbon-Free Fuel. In: ASME 2010 Internal combustion engine division fall technical conference, 2010, p. 111–7. http://dx.doi.org/10.1115/ICEF2010-35026.

[29] Reiter AJ, Kong S-C. Combustion and emissions characteristics of compression-ignition engine using dual ammonia-diesel fuel. Fuel 2011;90(1):87–97. http://dx.doi.org/10.1016/j.fuel.2010.07.055, URL https://www.sciencedirect.com/science/article/pii/S001623611000414X.

[30] Gross CW, Kong S-C. Performance characteristics of a compression-ignition engine using direct-injection ammonia–DME mixtures. Fuel 2013;103:1069–79. http://dx.doi.org/10.1016/j.fuel.2012.08.026, URL https://www.sciencedirect.com/science/article/pii/S001623611200662X.

[31] Ryu K, Zacharakis-Jutz GE, Kong S-C. Performance characteristics of compression-ignition engine using high concentration of ammonia mixed with dimethyl ether. Appl Energy 2014;113:488–99. http://dx.doi.org/10.1016/j.apenergy.2013.07.065, URL https://www.sciencedirect.com/science/article/pii/S0306261913006326.

[32] Mørch CS, Bjerre A, Gøttrup MP, Sorenson SC, Schramm J. Ammonia/hydrogen mixtures in an SI-engine: Engine performance and analysis of a proposed fuel system. Fuel 2011;90(2):854–64.

[33] Lhuillier C, Brequigny P, Contino F, Mounaïm-Rousselle C. Experimental study on ammonia/hydrogen/air combustion in spark ignition engine conditions. Fuel 2020;269:117448.

[34] Chiong M-C, Chong CT, Ng J-H, Mashruk S, Chong WWF, Samiran NA, et al. Advancements of combustion technologies in the ammonia-fuelled engines. Energy Convers Manage 2021;244:114460.

[35] Wang Y, Zhou X, Liu L. Theoretical investigation of the combustion performance of ammonia/hydrogen mixtures on a marine diesel engine. Int J Hydrogen Energy 2021;46(27):14805–12.

[36] Comotti M, Frigo S. Hydrogen generation system for ammonia–hydrogen fuelled internal combustion engines. Int J Hydrog 2015;40(33):10673–86. http://dx.doi.org/10.1016/j.ijhydene.2015.06.080, URL https://www.sciencedirect.com/science/article/pii/S0360319915015657.

[37] Mazzone S, Campbell A, Zhang G, García-García F. Ammonia cracking hollow fibre converter for on-board hydrogen production. Int J Hydrogen Energy 2021;46(76):37697–704. http://dx.doi.org/10.1016/j.ijhydene.2021.09.038, URL https://www.sciencedirect.com/science/article/pii/S0360319921035187.

[38] Wang Y, Zhou X, Liu L. Theoretical investigation of the combustion performance of ammonia/hydrogen mixtures on a marine diesel engine. Int J Hydrogen Energy 2021;46(27):14805–12. http://dx.doi.org/10.1016/j.ijhydene.2021.01.233, URL https://www.sciencedirect.com/science/article/pii/S0360319921004304.

[39] Xu X, Liu E, Zhu N, Liu F, Qian F. Review of the current status of ammonia-blended hydrogen fuel engine development. Energies 2022;15(3). http://dx.doi.org/10.3390/en15031023, URL https://www.mdpi.com/1996-1073/15/3/1023.

[40] Xu X, Liu E, Zhu N, Liu F, Qian F. Review of the current status of ammonia-blended hydrogen fuel engine development. Energies 2022;15(3):1023.

[41] Truedsson I, Foucher F, Pochet M, Jeanmart H, Contino F. Ammonia-hydrogen blends in homogeneous-charge compression-ignition engine. 2017, http://dx.doi.org/10.4271/2017-24-0087.

[42] Pochet M, Jeanmart H, Contino F. A 22: 1 compression ratio ammonia-hydrogen HCCI engine: combustion, load, and emission performances. Front Mech Eng 2020;6:43.

[43] Wang B, Yang C, Wang H, Hu D, Duan B, Wang Y. Study on injection strategy of ammonia/hydrogen dual fuel engine under different compression ratios. Fuel 2023;334:126666. http://dx.doi.org/10.1016/j.fuel.2022.126666, URL https://www.sciencedirect.com/science/article/pii/S0016236122034901.

[44] Wang B, Wang H, Duan B, Yang C, Hu D, Wang Y. Effect of ammonia/hydrogen mixture ratio on engine combustion and emission performance at different inlet temperatures. Energy 2023;272:127110.

[45] Wang B, Yang C, Wang H, Hu D, Wang Y. Effect of diesel-ignited ammonia/hydrogen mixture fuel combustion on engine combustion and emission performance. Fuel 2023;331:125865.

[46] Wang H, Wang B, Yang C, Hu D, Duan B, Wang Y. Study on dual injection strategy of diesel ignition ammonia/hydrogen mixture fuel engine. Fuel 2023;348:128526.

[47] Fukuzumi S, Yamada Y, Karlin KD. Hydrogen peroxide as a sustainable energy carrier: Electrocatalytic production of hydrogen peroxide and the fuel cell. Electrochim Acta 2012;82:493–511. http://dx.doi.org/10.1016/j.electacta.2012.03.132, Electrochemical Frontiers in Global Environment and Energy, URL https://www.sciencedirect.com/science/article/pii/S0013468612004847.

[48] Wernimont E, Ventura M, Garboden G, Mullens P. Past and present uses of rocket grade hydrogen peroxide. Gen Kinetics LLC Aliso Viejo, CA 1999;92656:680.

[49] Krishna B. Experimental investigation on CI engine with hydrogen peroxide as an alternate. Glob J Res Eng 2020;20(1):37–41.

[50] Fanz B, Roth P. Injection of a H2O2/water solution into the combustion chamber of a direct injection diesel engine and its effect on soot removal. Proc Combust Inst 2000;28(1):1219–25. http://dx.doi.org/10.1016/S0082-0784(00)80333-1, URL https://www.sciencedirect.com/science/article/pii/S0082078400803331.

[51] Yeom J-K, Jung S-H, Yoon J-H. An experimental study on the application of oxygenated fuel to diesel engines. Fuel 2019;248:262–77. http://dx.doi.org/10.1016/j.fuel.2018.12.131, URL https://www.sciencedirect.com/science/article/pii/S0016236118321999.

[52] Fernie O, Megaritis T, Ganippa LC, Tingas E-A. Numerical analysis of zero-carbon HCCI engine fuelled with steam diluted H2/H2O2 blends. Fuel 2022;326:125100. http://dx.doi.org/10.1016/j.fuel.2022.125100, URL https://www.sciencedirect.com/science/article/pii/S0016236122019408.

[53] Dimitrova ID, Megaritis T, Ganippa LC, Tingas E-A. Computational analysis of an HCCI engine fuelled with hydrogen/hydrogen peroxide blends. Int J Hydrogen Energy 2022;47(17):10083–96. http://dx.doi.org/10.1016/j.ijhydene.2022.01.093, URL https://www.sciencedirect.com/science/article/pii/S036031992200180X.

[54] Rabbani S, Manias DM, Kyritsis DC, Goussis DA. Dominant dynamics of n-butanol/air autoignition and the influence of additives. Combust Flame 2022;242:112173.

[55] Zhou A, Zhang C, Li Y, Li S, Yin P. Effect of hydrogen peroxide additive on the combustion and emission characteristics of an n-butanol homogeneous charge compression ignition engine. Energy 2019;169:572–9. http://dx.doi.org/10.1016/j.energy.2018.12.076, URL https://www.sciencedirect.com/science/article/pii/S0360544218324423.

[56] Khalil AT, Manias DM, Tingas E-A, Kyritsis DC, Goussis DA. Algorithmic analysis of chemical dynamics of the autoignition of NH3–H2O2/air mixtures. Energies 2019;12(23):4422.

[57] Shafiq O, Tingas E-A. Computational investigation of ammonia-hydrogen peroxide blends in HCCI engine mode. Int J Engine Res 2023;24(5):2279–94. http://dx.doi.org/10.1177/14680874221117686.

[58] Yang W, Al Khateeb AN, Kyritsis DC. The effect of hydrogen peroxide on NH3/O2 counterflow diffusion flames. Energies 2022;15(6):2216.

[59] Krishnamoorthi M, Malayalamurthi R, He Z, Kandasamy S. A review on low temperature combustion engines: Performance, combustion and emission characteristics. Renew Sustain Energy Rev 2019;116:109404.

[60] Dwarshala SKR, Rajakumar SS, Kummitha OR, Venkatesan EP, Veza I, Samuel OD. A review on recent developments of RCCI engines operated with alternative fuels. Energies 2023;16(7):3192.

[61] Agarwal AK, Singh AP, García A, Monsalve-Serrano J. Challenges and opportunities for application of reactivity-controlled compression ignition combustion in commercially viable transport engines. Prog Energy Combust Sci 2022;93:101028.

[62] Paykani A, Chehrmonavari H, Tsolakis A, Alger T, Northrop WF, Reitz RD. Synthesis gas as a fuel for internal combustion engines in transportation. Prog Energy Combust Sci 2022;90:100995.

[63] Li J, Yang W, Zhou D. Review on the management of RCCI engines. Renew Sustain Energy Rev 2017;69:65–79.

[64] Paykani A, Kakaee A-H, Rahnama P, Reitz RD. Progress and recent trends in reactivity-controlled compression ignition engines. Int J Engine Res 2016;17(5):481–524. http://dx.doi.org/10.1177/1468087415593013.

[65] Jain A, Krishnasamy A, V. P. Computational optimization of reactivity controlled compression ignition combustion to achieve high efficiency and clean combustion. Int J Engine Res 2021;22(7):2213–32. http://dx.doi.org/10.1177/1468087420931730.

[66] Urata Y, Taylor AMKP. Lean flames in practice. In: Swaminathan N, Bray KNC, editors. Turbulent premixed flames. Cambridge University Press; 2011, p. 244–364. http://dx.doi.org/10.1017/CBO9780511975226.005.

[67] Cordiner S, Gambino M, Iannaccone S, Rocco V, Scarcelli R. Numerical and experimental analysis of combustion and exhaust emissions in a dual-fuel diesel/natural gas engine. Energy Fuels 2008;22(3):1418–24. http://dx.doi.org/10.1021/ef7004755.

[68] CMCL innovations. 2023, https://cmclinnovations.com/. [Accessed 22 February 2023].

[69] Saxena MR, Maurya RK. Exergy analysis and investigation on effect of inlet valve closing temperature and hydrogen enrichment in syngas composition in an HCCI engine. Int J Hydrogen Energy 2023;48(8):3269–86.

[70] Coskun G, Demir U, Soyhan HS, Turkcan A, Ozsezen AN, Canakci M. An experimental and modeling study to investigate effects of different injection parameters on a direct injection HCCI combustion fueled with ethanol–gasoline fuel blends. Fuel 2018;215:879–91.

[71] Yasar H, Usta E, Demir U. Experimental and stochastic reactor modeling results of an HCCI engine fueled with primary reference fuel. Energy Fuels 2018;32(2):2497–505.

[72] Pasternak M, Mauss F, Perlman C, Lehtiniemi H. Aspects of 0D and 3D modeling of soot formation for diesel engines. Combust Sci Technol 2014;186(10–11):1517–35.

[73] CMCL innovations UK, kinetics & SRM engine suite. 2021.

[74] Pope SB. PDF methods for turbulent reactive flows. Prog Energy Combust Sci 1985;11(2):119–92.

[75] Curl RL. Dispersed phase mixing: I. Theory and effects in simple reactors. AIChE J 1963;9(2):175–81.

[76] Demir U, Yilmaz N, Coskun G, Soyhan HS. Evaluation of zero dimensional codes in simulating IC engines using primary reference fuel. Appl Therm Eng 2015;76:18–24.

[77] Maurya RK, Akhil N. Development of a new reduced hydrogen combustion mechanism with NOx and parametric study of hydrogen HCCI combustion using stochastic reactor model. Energy Convers Manage 2017;132:65–81. http://dx.doi.org/10.1016/j.enconman.2016.11.021, URL https://www.sciencedirect.com/science/article/pii/S0196890416310160.

[78] Zhang X, Moosakutty SP, Rajan RP, Younes M, Sarathy SM. Combustion chemistry of ammonia/hydrogen mixtures: Jet-stirred reactor measurements and comprehensive kinetic modeling. Combust Flame 2021;234:111653.

[79] Maurya RK, Mishra P. Parametric investigation on combustion and emissions characteristics of a dual fuel (natural gas port injection and diesel pilot injection) engine using 0-D SRM and 3D CFD approach. Fuel 2017;210:900–13. http://dx.doi.org/10.1016/j.fuel.2017.09.021, URL https://www.sciencedirect.com/science/article/pii/S0016236117311328.

[80] Wallington T, Wiesen P. N2O emissions from global transportation. Atmos Environ 2014;94:258–63.

[81] Greenhouse gas emissions standards and fuel efficiency standards for medium- and heavy-duty engines and vehicles— Phase 2. Regulatory impact analysis. Final rule. EPA-420-R-16-900. Washington, DC, USA: EPA, NHTSA; 2016.

[82] Zhang Y, Mathieu O, Petersen EL, Bourque G, Curran HJ. Assessing the predictions of a NOx kinetic mechanism on recent hydrogen and syngas experimental data. Combust Flame 2017;182:122–41.

[83] Wang S, Wang Z, Roberts WL. Measurements and simulations on effects of elevated pressure and strain rate on NOx emissions in laminar premixed NH3/CH4/air and NH3/H2/air flames. Fuel 2024;357:130036.

[84] Kim JH, Song JH, Ku JW, Kim YH, Kwon OC. Combustion characteristics of premixed ammonia-hydrogen/air flames in a swirl model combustor. Int J Hydrogen Energy 2023.

[85] Khateeb AA, Guiberti TF, Zhu X, Younes M, Jamal A, Roberts WL. Stability limits and NO emissions of technically-premixed ammonia-hydrogen-nitrogen-air swirl flames. Int J Hydrogen Energy 2020;45(41):22008–18.

[86] Hayakawa A, Arakawa Y, Mimoto R, Somarathne KKA, Kudo T, Kobayashi H. Experimental investigation of stabilization and emission characteristics of ammonia/air premixed flames in a swirl combustor. Int J Hydrogen Energy 2017;42(19):14010–8.

[87] Dinesh M, Kumar G. Effects of compression and mixing ratio on NH3/H2 fueled SI engine performance, combustion stability, and emission. Energy Convers Manag X 2022;15:100269.

[88] Zhang H, Li G, Long Y, Zhang Z, Wei W, Zhou M, et al. Numerical study on combustion and emission characteristics of a spark-ignition ammonia engine added with hydrogen-rich gas from exhaust-fuel reforming. Fuel 2023;332:125939.